



# Fluorescence nanoscopy in cell biology

Steffen J. Sahl<sup>1</sup>, Stefan W. Hell<sup>1–3</sup> and Stefan Jakobs<sup>1,4</sup>

**Abstract** | Fluorescence nanoscopy uniquely combines minimally invasive optical access to the internal nanoscale structure and dynamics of cells and tissues with molecular detection specificity. While the basic physical principles of ‘super-resolution’ imaging were discovered in the 1990s, with initial experimental demonstrations following in 2000, the broad application of super-resolution imaging to address cell-biological questions has only more recently emerged. Nanoscopy approaches have begun to facilitate discoveries in cell biology and to add new knowledge. One current direction for method improvement is the ambition to quantitatively account for each molecule under investigation and assess true molecular colocalization patterns via multi-colour analyses. In pursuing this goal, the labelling of individual molecules to enable their visualization has emerged as a central challenge. Extending nanoscale imaging into (sliced) tissue and whole-animal contexts is a further goal. In this Review we describe the successes to date and discuss current obstacles and possibilities for further development.

It is the promise of optical imaging in the 21st century to uncover the spatial organization of all molecules inside a cell and directly observe their interactions at the highest spatial and temporal levels of detail. As optics and chemistry join forces in fluorescence ‘nanoscopy’, the resolution revolution honoured by the 2014 Nobel Prize in Chemistry represents a paradigm shift in how we view the resolution problem in microscopy. Up to the end of the 20th century, microscopes discerned features through focusing. The focusing strength of the optical system (notably, the main lens, that is, the objective) alone dictated the resolution for well-corrected optics. In 1873, Abbe’s seminal theoretical analysis<sup>1</sup> of diffractive effects laid the ground for an enduring belief within the scientific community, namely, that optical microscopy resolution was to remain limited ([Supplementary information S1](#) (box)). This limitation is caused by the optical spot size in the lateral dimensions (in  $x$ - $y$ ), which cannot become any smaller upon focusing than the wavelength of light being used divided by twice the numerical aperture, yielding resolutions of  $\geq 200$  nm for visible light. The extent of the focal spot is even larger ( $\geq 500$  nm, and often more) in the axial direction (in  $z$ ).

Despite these apparent limits to the resolving power, the relatively benign, minimally invasive effects of light on living matter have made optical microscopy analysis a powerful tool for studies of structure and function at the subcellular level. However, an optical microscope with much higher resolution seemed unrealistic. Solutions eventually came from an unexpected reformulation of the resolution problem and by challenging its most basic assumptions<sup>2–5</sup>. The result has been fluorescence

nanoscopy<sup>6</sup>, which routinely obtains resolutions in the 20–50 nm range. This has enabled not only the cell surface but also the entirety of the cell interior to be examined at a level of nanoscale detail previously unattainable with light (FIGS 1,2).

In this Review, we describe selected applications of fluorescence nanoscopy, often also referred to as super-resolution microscopy, that have broken new ground in cell-biological research. We limit ourselves to the diffraction-unlimited concepts that have not just improved the resolution by a factor of two<sup>7</sup>, but have broken the resolution barrier altogether. These methods are being developed to reach down to the molecular scale (FIG. 3). As several aspects of nanoscopic imaging deserve specialized comprehensive reviews in their own right, we focus on a few illustrative examples of recent discoveries. We summarize molecular labelling considerations and constraints, approaches being used at the frontier of quantitative super-resolution imaging as well as advances in live-cell, tissue and *in vivo* nanoscopy.

## Breaking the diffraction barrier

Resolution in microscopy means the separation of distinct features. Typically, the goal is to separate molecules such as fluorophore-tagged proteins or nucleic acids found inside the cell. Irrespective of the microscope system, be it a widefield (epifluorescence) configuration or within the small focused laser spot of confocal laser scanning, all fluorophores illuminated by excitation light are excited quasi-simultaneously. The fluorescence emission of each fluorophore travels through the optical system at essentially the same time and is again subject to focusing

<sup>1</sup>Max Planck Institute for Biophysical Chemistry, Department of NanoBiophotonics, Am Fassberg 11, 37077 Göttingen, Germany.

<sup>2</sup>Max Planck Institute for Medical Research, Department of Optical Nanoscopy, Jahnstrasse 29, 69120 Heidelberg, Germany.

<sup>3</sup>German Cancer Research Center (DKFZ), BioQuant, Im Neuenheimer Feld 267, 69120 Heidelberg, Germany.

<sup>4</sup>University of Göttingen Medical Faculty, Department of Neurology, Robert-Koch-Strasse 40, 37075 Göttingen, Germany.

[steffen.sahl@mpibpc.mpg.de](mailto:steffen.sahl@mpibpc.mpg.de)  
[stefan.hell@mpibpc.mpg.de](mailto:stefan.hell@mpibpc.mpg.de)  
[sjakobs@gwdg.de](mailto:sjakobs@gwdg.de)

doi:10.1038/nrm.2017.71  
Published online 6 Sep 2017

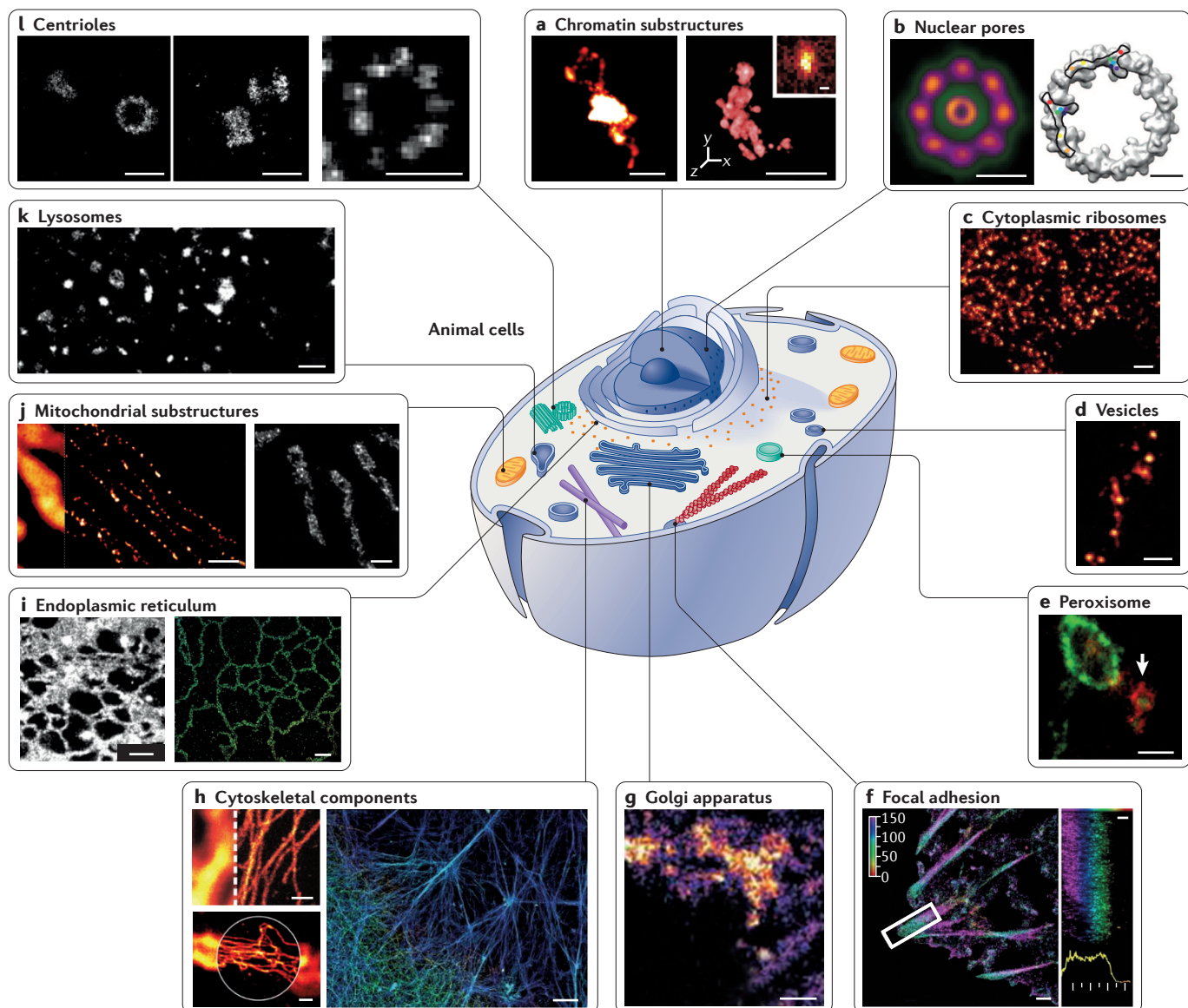


**Figure 1 | Dissecting animal cells with fluorescence nanoscopy.**  
**a** | Chromatin domains in *Drosophila melanogaster* nuclei. **b** | Nuclear pores. Left: averaged direct stochastic optical reconstruction microscopy (dSTORM) image showing the distribution of two nuclear pore (Nup) proteins in the nuclear pore complex (NPC) of *Xenopus laevis*; right: two possible arrangements for the Nup107-160 complexes based on ground state depletion with individual molecule return (GSDIM) data from a human NPC are traced within the electron density of the cytoplasmic ring of the nuclear pore. Scale bars: 100 nm (left), 25 nm (right). **c** | Cytoplasmic ribosomes in a human cell. **d** | Synaptic vesicles in living rat neurons. **e** | Human fibroblasts immunolabelled for the peroxisomal protein PEX5 (red) and the mitochondrial protein Tom20 (green). The arrow shows the colocalization of the two proteins. **f** | Focal adhesions in human cells. The colours indicate the vertical (z) coordinate of the labelled actin relative to the substrate. The panel on the right is a side view of the area indicated by the rectangle. **g** | Live nanoscopy of Golgi-derived vesicles. **h** | Nanoscopy of the cytoskeleton in a mammalian cell. Left, top: microtubules (in comparison with a confocal recording); left, bottom: vimentin (in comparison with a confocal recording); right: actin. The scale bar in the right panel is 2 μm. **i** | Live-cell nanoscopy imaging (left) and 4Pi single-molecule switching nanoscopy (right) of the endoplasmic reticulum in a mammalian cell. Scale bars: 1 μm. **j** | Nanoscopy images of mitochondria in human cells. Left: outer membrane protein Tom20 (in comparison with a confocal recording); right:  $F_1F_O$ ATPase in the inner

membrane. **k** | Lysosomes in a living mammalian cell. Scale bar: 1 μm. **l** | Centrioles in mammalian cells. Scale bar in the right panel: 250 nm. All scale bars are 500 nm unless stated otherwise. Part **a** is adapted with permission from REFS 208,209, Macmillan Publishers Limited. Part **b** (left) is adapted with permission from REF 80, Macmillan Publishers Limited, and (right) from REF 81. Reprinted with permission from AAAS. Part **c** is republished with permission of Rockefeller University Press, from REF. 210 (Three distinct ribosome assemblies modulated by translation are the building blocks of polysomes, Viero, G. et al., 208, 5, 2015); permission conveyed through Copyright Clearance Center, Inc. Part **d** is from REF 29. Reprinted with permission from AAAS. Part **e** is adapted from REF. 211, CC-BY 4.0. Part **f** is adapted with permission from REF. 212, Macmillan Publishers Limited. Part **g** is from REF 213 (Erdmann, R. S. et al. Superresolution imaging of the Golgi in live cells with a bioorthogonal ceramide probe. *Angew. Chem. Int. Ed. Engl.* 2014, 53, 10242–10246). Copyright Wiley-VCH Verlag GmbH & Co. KGaA. Reproduced with permission. Part **h** is adapted with permission from REFS 63,214, Macmillan Publishers Limited, and unpublished observations (S.J.). Parts **i** (left) and **k** are adapted with permission from REF. 136, National Academy of Sciences. Part **i** (right) is adapted from REF. 51, CC-BY 3.0. Part **j** is reprinted (adapted) with permission from REF. 46 (Schmidt, R. et al. Mitochondrial cristae revealed with focused light. *Nano Lett.* 9, 2508–2510 (2009)). Copyright (2009) American Chemical Society. Part **l** (left) is adapted from REF. 215, CC-BY 3.0, and (right) from REF. 216, The American Society for Cell Biology.

**Numerical aperture (NA).** Measure of the opening angle under which light is collected by an objective lens. The NA ( $n \cdot \sin\alpha$ , with  $n$  being the refractive index and  $\alpha$  the semi-aperture angle) determines the tightest focusing possible and thus establishes the resolution of diffraction-limited microscopy.

#### Fluorophore states

States with defined properties. In the context of nanoscopy, useful pairs of states are pairs for which one of them gives a signal ('on'), whereas the other one does not ('off'), as this allows fluorophores to be distinguished even when they are located in closer proximity to each other than the diffraction limit.

#### Stimulated emission depletion (STED)

The stimulated emission process transfers the excited fluorophore to its ground state. The stimulating photon induces the generation of a stimulated identical photon, which is not detected. The STED light thus exits the specimen, providing a clean fluorophore off-switch. The near-infrared light used in STED is hardly absorbed by the cell.

**Reversible saturable/switchable optical linear (fluorescence) transitions (RESOLFT).** The general conceptual framework for coordinate-targeted nanoscopy. The term is mostly used in reference to approaches using reversibly switchable fluorescent proteins (RSFPs, see below) or photochromic organic compounds.

**Photo-activated localization microscopy/stochastic optical reconstruction microscopy (PALM/STORM).** Coordinate-stochastic nanoscopy concepts based on the switching and localization of single molecules. Conceptually similar techniques include fluorescent PALM (fPALM) and ground state depletion with individual molecule return (GSDIM).

and diffraction as an image is formed on a camera (in the case of a widefield microscope) or signals are registered by a point detector (in beam-scanning systems). All fluorophores residing in closer proximity to each other than the diffraction limit are thus inseparable; they are excited together, they emit together, and their emissions diffract together and are detected together. This limitation seemed impossible to surpass. The key to nanoscopy<sup>5,6</sup> is to render the molecules themselves discernible for a short period of time, preventing different molecules within the same diffraction region from being detected together. Molecular transitions (switching) between two fluorophore states, typically a fluorescent 'on' state and a dark, non-fluorescent 'off' state<sup>2–4</sup>, allow the limiting role of diffraction to be neutralized. Most nanoscopy variants switch off the fluorescence ability of the majority of the fluorophores within a diffraction region and record few or even single on-state molecules at a time (FIG. 3a–c). Then, other fluorophores are transitioned from the off to the on state, and their signals are read out, a process that is repeated until a full description of the spatial arrangement of molecules is obtained. The on-off separation (FIG. 3d) can be implemented in two ways.

In methods such as stimulated emission depletion (STED)<sup>2,8–11</sup> and reversible saturable/switchable optical linear (fluorescence) transitions (RESOLFT)<sup>12–14</sup> microscopy (FIG. 3a), light is applied to induce transitions between two states and to switch fluorophores on and off at defined spatial coordinates (coordinate-targeted nanoscopy). In this approach, the light features intensity minima (one, several or many), ideally with zero intensity. At these minima (zeros), there is no off-switching, and the fluorophores in the on state can fluoresce. The reverse scenario, namely, on-switching everywhere but at the minima, can also be implemented. For STED and RESOLFT point-scanning implementations in 2D, the minimum is at the centre of a doughnut-shaped light focus (FIG. 3a).

The methods (fluorescence) photo-activated localization microscopy/stochastic optical reconstruction microscopy ((f)PALM/STORM)<sup>15–18</sup> (FIG. 3b) stochastically establish the on state at the single-molecule level, so that only a single fluorophore within a distance larger than the diffraction limit is able to emit. Each fluorophore can then be separately localized (coordinate-stochastic nanoscopy). Currently, most applications of the PALM/STORM concept rely on fluorophore blinking in the presence of excitation light, as in the method termed ground state depletion with individual molecule return<sup>19–21</sup>, also called direct STORM (dSTORM)<sup>22</sup>. While essentially all fluorophores blink, only fluorophores with suitable switching (that is, blinking) kinetics give good PALM/STORM images<sup>23</sup>. Another powerful variant of the stochastic state-switching concept is points accumulation for imaging in nanoscale topography (PAINT)<sup>24</sup>. In PAINT, single fluorophores, which reversibly attach to the target structure, are turned 'on' and detected, whereas all other unbound, mobile fluorophores remain 'off' and undetected. In these coordinate-stochastic methods, molecule positions are inferred from the photons registered from single fluorophores. Switching the fluorescence

ability at the single-molecule level<sup>25</sup> is a powerful and efficient way to bring about the on-off state difference, but the precision of localization does not scale favourably with the number of photons ( $N$ ) collected ( $\sim 1/\sqrt{N}$ ). Large numbers of photons are needed to determine the position of each fluorophore with very high precision. In most cases, however, the total budget of photons from a single fluorophore is rather limited owing to photobleaching.

The concept referred to as nanoscopy with minimal photon fluxes (MINFLUX)<sup>26</sup> (FIG. 3c) addresses this limitation imposed by photon budget and achieves the highest levels of localization precision of all nanoscopy approaches, with much fewer photons. MINFLUX nanoscopy achieved a 1 nm resolution in examination of DNA origami structures by combining the strengths of coordinate-targeted and -stochastic approaches. This approach utilizes the stochastic on-off switching of individual molecules to infer their positions by placing an excitation-light intensity minimum at targeted positions to measure signals<sup>26</sup>. Concepts such as multiple off-state transitions for nanoscopy<sup>27</sup> and MINFIELD<sup>28</sup> can help push resolution, signal, image contrast and/or temporal sampling while reducing the light dose to a sample. We predict that further variants of MINFLUX will be developed to examine fast local dynamics<sup>29</sup>, including highly parallelized versions of the concept (with many minima targeting many coordinates simultaneously) for larger fields of view.

We note that several useful diffraction-limited developments in microscopy that are not discussed in this review have improved the contrast, the optical sectioning and, to some extent, the resolution compared with conventional fluorescence microscopy. Among these are the seminal realization of confocal detection<sup>30</sup>, deconvolution approaches and the implementation of structured illumination microscopy (SIM)<sup>7</sup>, as well as approaches such as AiryScan<sup>31,32</sup> or lattice light-sheet microscopy<sup>33</sup>. SIM has clear merits as a tool for live-cell imaging<sup>34–37</sup>, although this technique is diffraction-limited and has only an approximate 2-fold increase in resolution compared with epifluorescence. Following earlier ideas of RESOLFT microscopy<sup>4,12–14</sup>, a technique combining SIM with reversible photoswitching, termed patterned-activation nonlinear SIM (PA NL-SIM),<sup>38</sup> essentially reduced the switching contrast to the bearable minimum by incomplete on- and off-switching, allowing faster imaging. As a consequence of the requirement to mathematically reconstruct an image in frequency space from raw data, artefacts have remained a problem in NL-SIM<sup>39</sup>. Super-resolution optical fluctuation imaging<sup>40,41</sup> achieves resolution enhancement by analysing fluorescence fluctuations over time and extracting additional spatial information. However, the resolution levels that can be reliably achieved using this method are variable, and there is a need for further work to quantify the attainable resolution gain in cellular imaging, which is typically 2- to 3-fold over the classical diffraction limit. An intriguing approach also not discussed here is the physical expansion of fixed specimens<sup>42</sup> using swellable polymer networks, which allows the visualization of finer details with fluorescence microscopy at conventional resolution.

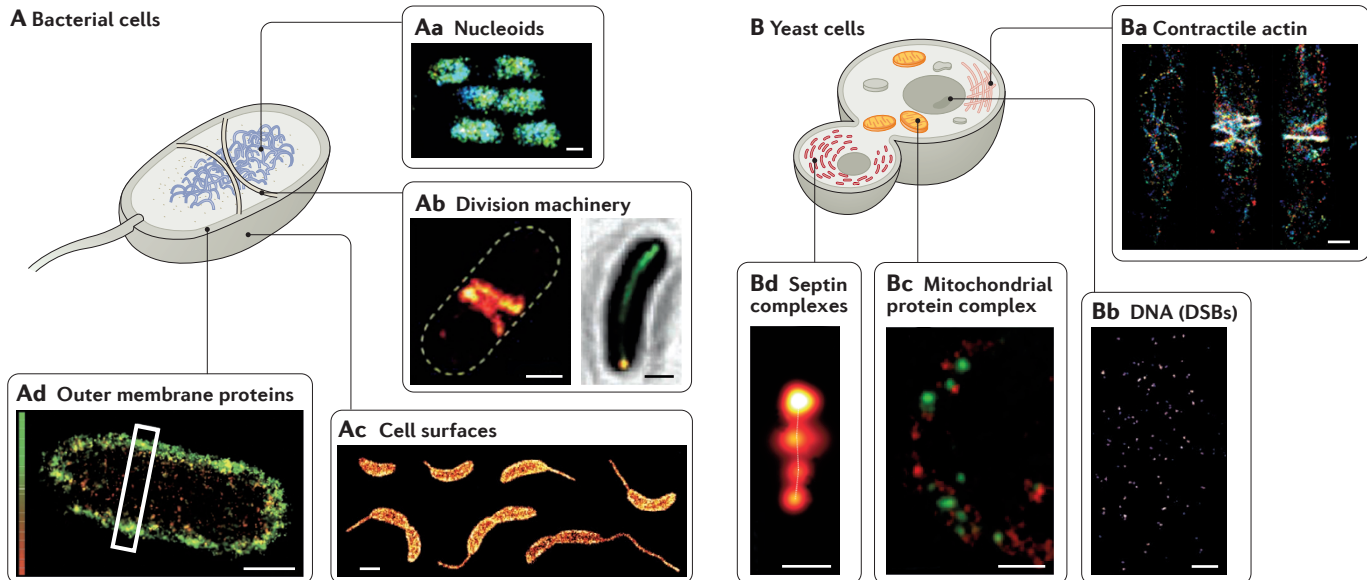


**Figure 2 | Examples of fluorescence nanoscopy in bacteria and yeast.** **A** | Bacterial cells. **Aa** | Nucleoids in living *Escherichia coli* cells. **Ab** | Left panel: fixed *E. coli* cell expressing FtsZ, which is required for cell division. Right panel: partitioning apparatus of *Caulobacter crescentus*. **Ac** | 3D super-resolution images of the outer surfaces of *C. crescentus* cells. Scale bar: 1 μm. **Ad** | Outer membrane proteins in *E. coli*. **B** | Yeast cells. **Ba** | Contractile actin rings in fission yeast. **Bb** | Budding yeast cell stained for Rad51, which is required to repair DNA double-strand breaks (DSBs). **Bc** | Dual-colour image of mitochondria in a budding yeast cell showing nucleoid (red)–protein (green) complexes. **Bd** | Septin arrangement in the fungus *Ashbya gossypii* resolved with nanoscopy. All scale bars are 500 nm unless stated otherwise. Part **Aa** is from REF. 217. Reprinted with permission from AAAS. Part **Ab** (right) is adapted with permission from REF. 218, Macmillan Publishers Limited, and (left) from REF. 219, CC-BY 3.0. Part **Ac** is adapted with permission from REF. 220, American Chemical Society. Part **Ad** is adapted from REF. 221, CC-BY 3.0. Part **Ba** is adapted with permission from REF. 222, National Academy of Sciences. Part **Bb** is adapted from REF. 223, CC-BY 3.0. Part **Bc** is adapted from REF. 128, CC-BY 3.0. Part **Bd** is reprinted (adapted) with permission from REF. 224. Copyright (2015) American Chemical Society.

Points accumulation for imaging in nanoscale topography (PAINT). A coordinate-stochastic nanoscopy concept based on separating fluorophores by registering only the bound ones ('on'), with the diffusing fluorophores remaining undetected ('off').

Nanoscopy with minimal photon fluxes (MINFLUX). A concept that allows precise localization of fluorophores with minimal fluxes of emitted photons. MINFLUX nanoscopy combines coordinate-targeted and coordinate-stochastic aspects.

Multiple off-state transitions for nanoscopy (MOST). A concept that synergistically combines two or more state-transfer mechanisms to, for example, protect the fluorophore from pathways related to photobleaching and improve signal-to-background in coordinate-targeted nanoscopy.

### Performance of nanoscopy

Many of the earliest experimental nanoscopy reports relied on thin, flat and often chemically fixed cells<sup>8,15,18</sup>, in which a 2D resolution gain was sufficient to demonstrate the advantage of improved resolution.

A critical development has been the extension of both coordinate-targeted and coordinate-stochastic nanoscopy to the third spatial dimension. In the case of STED and RESOLFT, similar optical strategies that switch off fluorophores laterally to the centre of a doughnut-shaped light focus can be used to additionally disallow fluorescence along the z direction above and below the focal plane<sup>43</sup>. The use of two opposing objective lenses of high numerical aperture in a so-called 4Pi arrangement<sup>44</sup> provides the highest axial resolutions, which can become equal to (or even better than) the lateral resolution. The result is an isotropic nanoscale resolution, albeit at the cost of higher optical sophistication and more elaborate sample preparation. The 4Pi strategy has been applied in isotropic STED (isoSTED)<sup>45–47</sup>, isoRESOLFT<sup>48</sup> and widefield PALM/STORM-type nanoscopy<sup>49–51</sup> to achieve the ultimate levels of 3D resolution. The widefield readout in coordinate-stochastic nanoscopy has allowed the development of other approaches that provide the 3D positions of each registered single molecule. These approaches include nanoscopy with astigmatism<sup>52</sup> and bi-plane imaging<sup>53</sup>,

as well as methods such as double-helix imaging<sup>54–57</sup> or Airy-beam detection<sup>58</sup> that allow larger (>1 μm) axial ranges. Despite these developments, the physical limits of encoding information in single-molecule images have not yet been reached<sup>59–61</sup>.

Comparing the resolution performance of different nanoscopy methods (FIG. 3e), we note that both coordinate-targeted and coordinate-stochastic approaches, and in particular MINFLUX, can conceptually reach a molecular-scale (<5 nm) resolution. Some experiments have already shown an ~10 nm resolution in cellular nanoscopy<sup>50,51,62,63</sup>. In most practical cellular applications, however, this level of resolution is often not achieved. The difference between the theoretically achievable and practical resolution can largely be attributed to the use of non-optimal fluorophores and labelling. Molecular brightness, photostability and photoswitching properties (for example, kinetics and switching fatigue) are key parameters contributing to resolution performance and the attainable contrast. Fluorophores for coordinate-targeted concepts have to undergo more on-off switching cycles than those for coordinate-stochastic approaches, which require more fluorophore emission cycles. Much of the progress in nanoscopy will eventually depend on the identification of improved switchable fluorophores and concepts that can help overcome limitations related to signal yield and other performance aspects<sup>27,28,62,64</sup>.

**MINFIELD**

A method for increasing the signal (photobleaching reduction) in coordinate-targeted nanoscopy. Using scan fields below the diffraction limit around an intensity minimum (for example, at the centre of a doughnut shape) avoids subjecting the fluorophores to the excess intensities of switching light at the maxima of the off-switching pattern.

**Optical sectioning**

Used to obtain an image with sufficient contrast that is not compromised by fluorescence originating in other axial planes of the specimen. For example, a confocal pinhole can act to reject the out-of-plane background. Other sectioning strategies include selective excitation or photoactivation by multi-photon absorption or light sheets.

**Deconvolution**

An algorithm to reverse the effects of convolution in the image formation process. By removing the optical blur, a sharper image is computed based on the (ideally) exact knowledge of the blurring (formalized by the so-called point spread function (PSF)). Because knowledge of this PSF is in practice imperfect, and registered images are compromised by noise, artefacts can easily arise in the deconvolution process. Deconvolution is not equivalent to methods that actually improve the spatial resolution by a (on-off) state transition.

**Structured illumination microscopy**

(SIM). A diffraction-limited method that produces up to 2-fold improved resolution and requires the acquisition of several images of a specimen with shifted illumination patterns and computation of a reconstructed image. Further improvements in resolution can be realized if on-off transitions (as in reversible saturable/switchable optical linear (fluorescence) transitions) are incorporated.

Considerable practical differences exist among the available nanoscopy techniques in terms of axial sectioning ability, attainable imaging depth and acquisition speed. In general, single-molecule stochastic methods fare less well in scenarios with high background signals, and it generally takes significantly longer to read out molecules one by one owing to the need for largely non-overlapping diffraction spots of isolated molecules on the camera<sup>65,66</sup>. Coordinate-targeted scanning methods can quickly survey signals at pre-set coordinates and have achieved very fast imaging within small regions of interest, allowing recordings at video-rate speed<sup>29</sup> and even down to the millisecond scale<sup>67</sup>. Most beam-scanning STED and RESOLFT implementations harness confocal pinholes. In many scenarios, confocality is a major advantage owing to the inherent optical sectioning and background suppression.

**Nanoscopy as a tool for discovery**

Overcoming the initial hurdles of limited access to pioneering instruments in only a small number of laboratories, adoption of fluorescence nanoscopy has picked up quickly, not least because of commercialization, a trend that is still accelerating. Nanoscopy has been successfully used to probe the internal structures of both eukaryotic and prokaryotic cells (FIGS 1,2), and the number of studies investigating new biological questions and surveying previously unattainable scales has rapidly increased.

Different areas of cell biology have adopted nanoscopy at different speeds. Whereas virology and microbiology were quick to use these approaches, in plant biology, a field with very strong roots in microscopy, only a few nanoscopy studies have been reported<sup>68</sup>. Initially, most nanoscopy studies utilized mammalian cells grown on cover glass. However, as new techniques developed and instrument availability expanded, nanoscopy has been increasingly used to investigate nanoscale structures in cells grown in more complex environments such as 3D cell cultures and biofilms as well as in tissues and even living animals. Nanoscopy has been used to address questions in fields such as immunology<sup>69</sup>, signalling<sup>70</sup>, virology<sup>71–75</sup>, bacteriology<sup>76</sup> and cancer biology<sup>77</sup>. The first reports of using nanoscopy on tissues from human patients have also appeared<sup>78,79</sup>, pointing to exciting future possibilities in medical diagnostics.

Nanoscopy has also been applied to study the detailed architecture of molecular machines and complexes within cells. Notably, images of labelled nuclear pore complexes (NPCs) have been analysed by single-particle averaging, a method well established in electron tomography, to map specific proteins within these structures<sup>80,81</sup>. On the basis of images of thousands of NPCs, it has been possible to determine the average positions of individual proteins of the Nup107-160 subcomplex with a precision of well below 1 nm, shedding light on the molecular architecture of this pore<sup>81</sup>. This approach has even been transferred to reconstruct 3D datasets<sup>82</sup>, and similar strategies have also been used to investigate symmetric structures such as primary cilia<sup>83</sup> or herpes simplex viruses<sup>84</sup>.

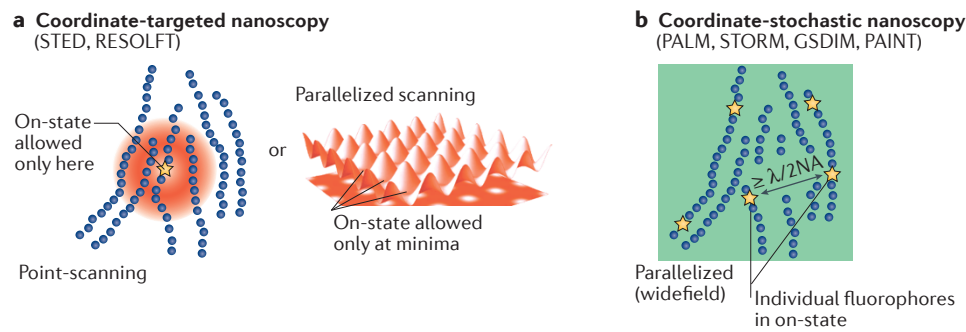
**Examples of nanoscopy in cell biology**

Nanoscopy has come of age, and its benefits typically manifest in combination with other experimental approaches. As of early 2017, the keywords ‘nanoscopy’ and ‘super-resolution microscopy’ together result in more than 16,000 hits in a Web of Science database search. Hence, given the wealth of studies using nanoscopy, it would be an all but impossible undertaking to try to appropriately cover all these applications. We refer to expert reviews on various subfields but will briefly discuss some important findings in two fields that have been at the focus of nanoscopy since its beginnings, namely, neurobiology and mitochondrial biology.

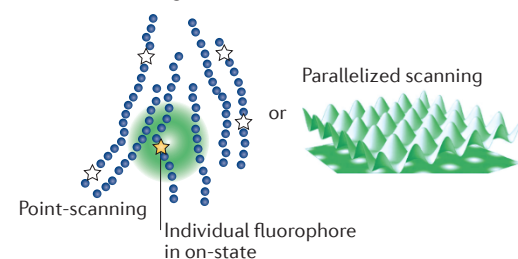
**Nanoscopy of neurons.** In the early days of nanoscopy, the fluorescently labelled cytoskeleton was primarily used as a convenient cellular structure to determine the resolving power of an instrument. It came as a surprise when it was shown, first in neuronal axons<sup>85</sup> and later also in dendrites<sup>86,87</sup> and spine necks<sup>88,89</sup>, that short actin filaments capped by adducin are bridged by spectrin tetramers to form a ~190-nm periodic ring-like structure underneath the plasma membrane<sup>85,90,91</sup> (FIG. 4a). This periodic lattice has been visualized in both chemically fixed and living cells in virtually every neuron type as well as in glial cells<sup>92–94</sup>, suggesting that it is a more general feature of the cytoskeleton in cells of the nervous system. The periodic scaffold forms a diffusion barrier<sup>95</sup> and regulates the positioning of other proteins that all exhibit the same periodicity, such as ankyrins, sodium and potassium channels, and adhesion molecules<sup>85,86,90,96</sup>. This periodicity is even coordinated between axon and glial cells at the nodes of Ranvier<sup>96</sup> (FIG. 4b). Remarkably, the periodic actin structure has eluded visualization by electron microscopy. Hence, this repetitive organization of the cytoskeleton in neurons found by STORM and STED is a bona fide example of a subcellular structure discovered by fluorescence nanoscopy.

As learning and memory are encoded in large part by the presynapses and postsynapses established by transmitting and receiving neurons, an understanding of brain function requires detailed insights into the architecture of these structures. In an attempt to obtain a global view of the structure of the presynapse, synaptic boutons containing the entire synaptic machinery were purified from rat brains and analysed by quantitative western blotting, mass spectrometry, electron microscopy and nanoscopy<sup>97</sup>. This led to the generation of an ‘average’ synapse model composed of the merged datasets. Although many details are missing from this model or need further verification, it provides some insight into the enormous nanoscale complexity of structures such as the synapse.

Most nanoscopy studies on synapses have concentrated on the presynaptic active zones (release sites) and the dendritic spines, which contain the postsynaptic machinery<sup>98,99</sup>. The protein-rich active zones are often smaller than the diffraction limit. A clearer picture of how molecular scaffolds and machineries are organized in sub-synaptic nanodomains is emerging, although the data are far from providing a complete image of



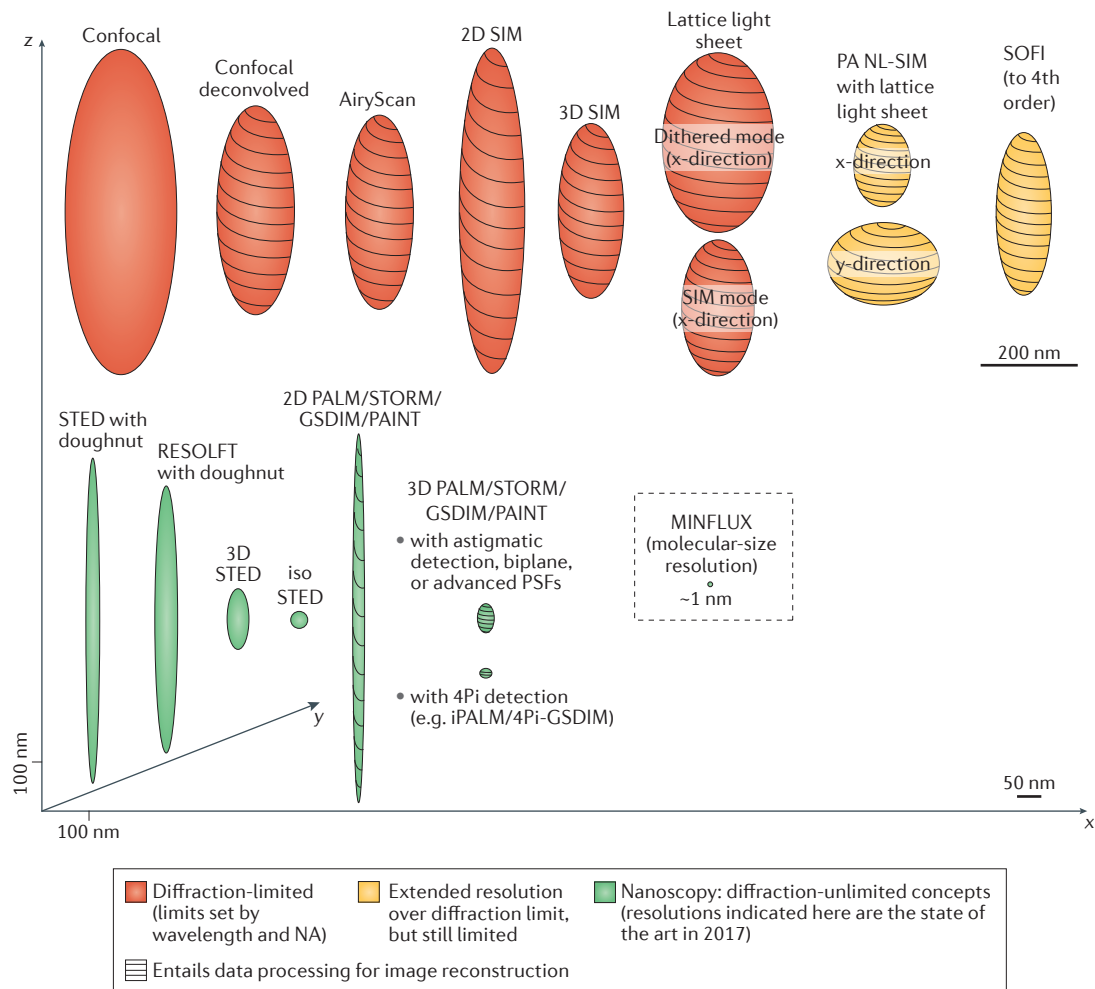
**c Coordinate-stochastic on-off switching and coordinate-targeted readout (MINFLUX)**



**d State switching key to breaking diffraction barrier**



**e Routine 3D resolution levels obtained for recordings of cell interiors**



**AiryScan**

A diffraction-limited method that combines conventional confocal laser scanning microscopy with fast widefield detection or other detector designs to achieve close to a doubling of resolution after mathematical processing. Also known as image scanning microscopy (ISM).

**Lattice light-sheet microscopy**

A diffraction-limited method that uses a structured light sheet to excite fluorescence in successive planes of a specimen, generating a time series of 3D images that can provide information about dynamic biological processes.

all proteins<sup>10,100–111</sup>. Nanoscopy has contributed to the identification of long-range organization across the synaptic cleft and has revealed molecular components that are co-aligned in the pre- and postsynapse. These so-called nanocolumn arrangements may facilitate effective synaptic communication<sup>112</sup> (FIG. 4c).

Dendritic spines are specialized micron-sized membrane protrusions harbouring the postsynaptic machinery. These spines contain a highly branched actin cytoskeleton network, which influences their shape. Live-cell nanoscopy imaging has revealed the high level of heterogeneity and pronounced dynamics of this network<sup>113–115</sup>. Remarkably, STED nanoscopy in combination with fluorescence recovery after photo-bleaching (FRAP) experiments and electrophysiology allowed the simultaneous measurement of spine-neck geometry and the movements of molecules in and out of the spines with high temporal resolution<sup>116–118</sup> (FIG. 4d). These data showed that the biochemical compartmentalization of the spines, which separates them from dendrites, critically depends on spine-neck width<sup>118</sup>.

This compartmentalization appears to be a major factor in the fine-tuning of synaptic strength, which is crucial for the computational power of neurons.

Neurodegenerative disorders, such as Parkinson disease, Alzheimer disease and Huntington disease, are characterized by aberrant accumulations of proteins or peptides in the brain, with subsequent neuronal death and the loss of motor and/or cognitive function. A crucial and unresolved question is which of the polymorphic aggregation states elicit toxic cellular responses and by which mechanisms. Nanoscopy is at the stage of being able to directly visualize protein aggregation, such as aggregate nucleation events and fibril formation<sup>119,120</sup>, and to carry out such studies in cells<sup>121–123</sup> (FIG. 4e). We expect that the ability to selectively co-visualize the action of cellular protein quality-control and degradation systems, such as the ubiquitin–proteasome pathway, autophagy-mediated degradation and chaperone networks, will add new information about which aggregation species are resilient to degradation and drive toxic cascades. As an example of the capabilities of nanoscopy, it has been demonstrated that exogenous addition of a chaperonin subunit attenuates the formation of both huntingtin (Htt) inclusion bodies and other smaller fibrillar Htt species present in the cytosol of neuronal model cells<sup>124,125</sup>, potentially enabling the development of pharmaceutical strategies that can interfere with these aggregation processes. Nanoscopy has also provided information on the interactions of larger Htt aggregates with transcription factors, suggesting that these aggregates exert some of their cytotoxic effects by interfering with gene transcription<sup>126</sup>.

**Nanoscopy of mitochondria.** Like the cytoskeleton, mitochondria have been at the focus of nanoscopy since its beginnings<sup>15,45,46,127–131</sup>. In particular, antibodies against Tom20 and Tom22, both membrane-spanning receptor proteins of the translocase of the outer membrane (TOM) complex, which is found in clusters on the surfaces of mitochondria, were extremely useful in early studies and often applied to demonstrate the resolving power of nanoscopy instruments<sup>51,127,132–134</sup>.

Seminal electron microscopy work on mitochondria performed in the early 1950s revealed that these organelles feature a smooth outer membrane and a highly convoluted inner membrane that forms folds referred to as cristae, which project into the mitochondrial interior<sup>135</sup>. Cristae have been repeatedly imaged using nanoscopy<sup>45,46,136,137</sup>, although they remain a challenging target because of their small size and elaborate 3D structure. Several studies have shown that not only the architecture and orientation of the cristae membranes but also the protein distributions within the membranes are adapted to the cellular environment<sup>138,139</sup>. Detailed measurements of the movement of proteins within the inner membrane have proved difficult, as diffraction-limited FRAP and related approaches inherently average across sub-domains such as individual cristae, making the analysis of FRAP data from inner membrane proteins challenging<sup>140,141</sup>. Using elements of single-molecule tracking and coordinate-stochastic nanoscopy, quantitative data on

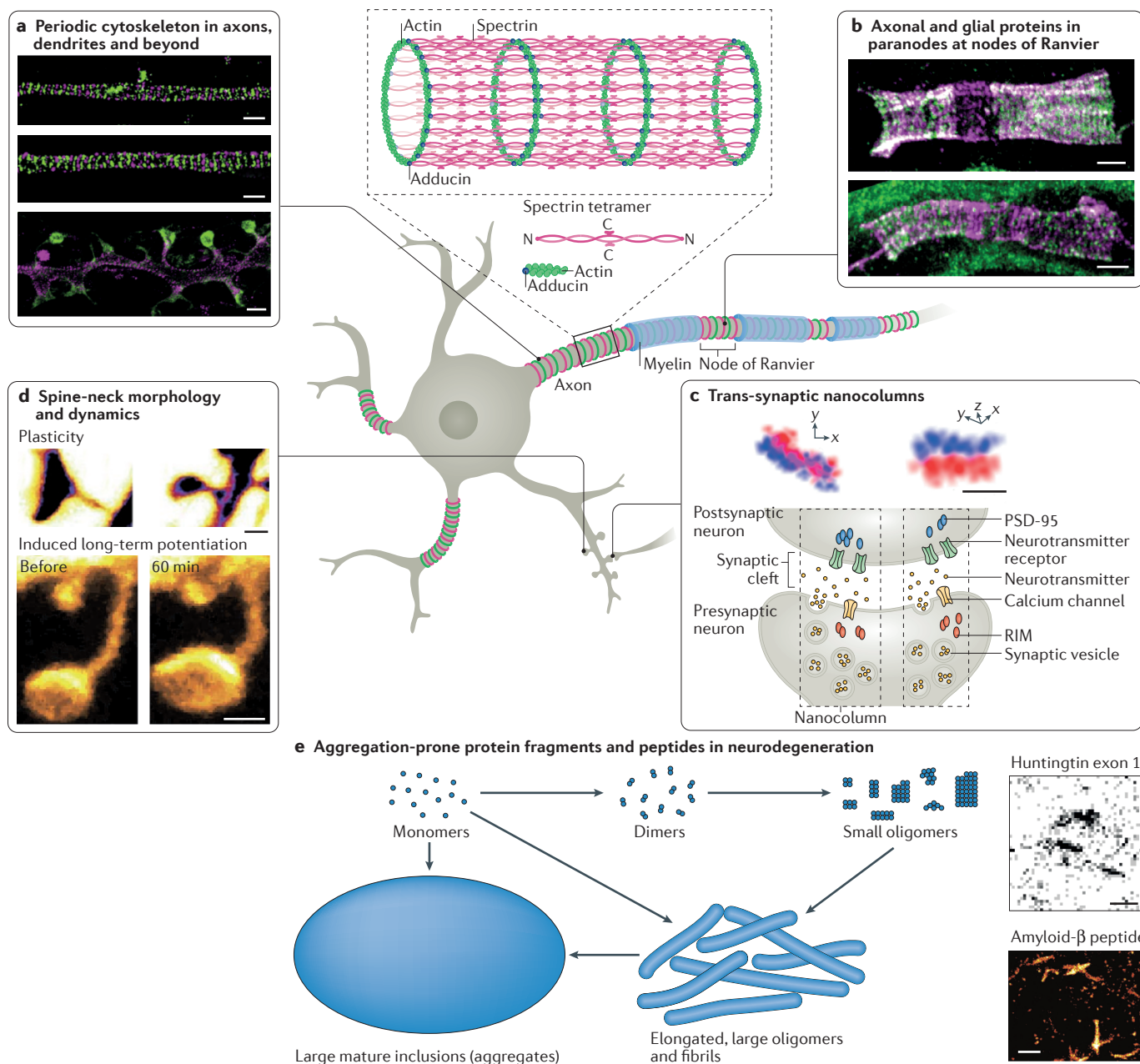
**Figure 3 | The state of the art in fluorescence nanoscopy: basic working principles and comparisons of 3D resolution.** **a–c** Major classes of diffraction-unlimited fluorescence nanoscopy concepts. **a** In stimulated emission depletion (STED) and reversible saturable/switchable optical linear fluorescence transitions (RESOLFT) nanoscopy, a specific light pattern (red, doughnut-shaped) is used to switch the fluorescence ability of fluorophores ‘off’, whereas fluorophores remain ‘on’ only at the intensity minima (shown by yellow star). This approach can also be parallelized (red, periodic pattern). **b** In methods such as photo-activated localization microscopy (PALM), stochastic optical reconstruction microscopy (STORM), ground state depletion with individual molecule return (GSDIM) and points accumulation for imaging in nanoscale topography (PAINT), single on-state fluorophores are established at distances larger than the diffraction limit ( $\lambda/2NA$ , where  $\lambda$  is the wavelength, and NA is the numerical aperture of the objective). **c** In MINFLUX (nanoscopy with minimal photon fluxes), single fluorophores can be localized at the nanometre scale with minimal photon numbers because their position is inferred from the positioning of the intensity minimum of the light pattern used for excitation. **d** All diffraction-unlimited super-resolution concepts utilize fluorophore state transitions to render adjacent molecules within a common diffraction zone transiently discernible. Transitions between a bright light-emitting on state and a dark off state have proved the most effective and have allowed the diffraction barrier to be broken. **e** Comparison of routine levels of 3D resolution obtained using different microscopy techniques for cellular imaging. The ellipsoids indicate the lateral (x, y) and axial (z) resolution levels of the listed methods. Each ellipsoid can be interpreted as an uncertainty range from where detected photons originate. Imaging methods with limited resolution owing to diffraction are shown in red (assumed emission wavelength: ~650 nm). The conceptually diffraction-unlimited methods (that is, the nanoscopy methods) are shown in green. The methods indicated in yellow have been shown to feature extended resolution over the diffraction limit, but their practical applicability and/or reliability with respect to resolution need to be further explored. The indicated resolutions have been repeatedly demonstrated in cell-imaging applications and do not simply represent ultimate or best values provided in the literature. The resolutions shown for lattice light-sheet microscopy and patterned-activation nonlinear structured illumination microscopy (PA NL-SIM) were taken from REFS 33,38. Confocal RESOLFT resolutions are shown for green fluorescent proteins. The resolution of diffraction-unlimited nanoscopy is limited by the photostabilities and physical sizes (compare with FIG. 6) of the marker fluorophores as well as the attachment strategy. The recently demonstrated MINFLUX concept (see part c) fundamentally addresses the limited photon budget and promises further advances in resolution and recording speed. The dithered mode in the ellipsoid corresponding to lattice light-sheet microscopy involves the rapid scanning of the light sheet along the x-axis, with only one image being recorded per z-plane. iPALM, interferometric photoactivated localization microscopy; isoSTED, isotropic STED; NA, numerical aperture; PSF, point spread function; SIM, structured illumination microscopy; SOFI, super-resolution optical fluctuation imaging.

Super-resolution optical fluctuation imaging (SOFI). A method that analyses on-off fluctuations of fluorescence signals (but not strictly at the single-molecule level as in photo-activated localization microscopy and stochastic optical reconstruction microscopy) by examining correlations in time to improve resolution typically 2- to 3-fold in comparison with epifluorescence.

the mobility of proteins within subcompartments of the mitochondrial inner membrane were obtained<sup>142</sup> (FIG. 5a). The data provide experimental evidence for the concept that cristae membranes act as diffusion-restricting micro-compartments and open novel possibilities for studying inner-mitochondrial dynamics.

Although mitochondria are best known for their role as the 'power houses' of the cell, they are also key players in executing apoptosis, a tightly regulated suicide programme in eukaryotic cells<sup>143</sup>. Upon apoptosis initiation, the pro-apoptotic proteins BCL-2-associated X protein (Bax) and BCL-2 antagonist or killer (Bak) accumulate in clusters on the mitochondrial outer membrane and thereby open the membrane to facilitate the release of cytochrome *c* into the cytosol<sup>144</sup>. The released cytochrome *c* then initiates a signalling cascade that

ultimately results in cell death. While the key roles of Bax and Bak in mitochondrial outer membrane permeabilization have been known since the late 1990s, the structural mechanism of membrane rupture remained elusive. In 2016, two independent studies using STED and PALM nanoscopy revisited this problem by visualizing Bax in apoptotic cells<sup>145,146</sup>. Both studies reported the formation of unexpected Bax assemblies. The STED study<sup>145</sup>, imaging endogenous Bax using immunofluorescence, demonstrated that Bax molecules in the mitochondrial outer membrane assemble into rings whose interiors are devoid of outer membrane proteins (FIG. 5b). This finding strongly suggested that several Bax molecules form a pore in the outer membrane. Remarkably, a subsequent study using cryo-electron microscopy of Bax in artificial membranes further



**4Pi**

Optical arrangement for coherent excitation and/or collection of fluorescence emissions featuring two juxtaposed lenses of high numerical aperture to expand the solid angle as much as possible, which enables very high axial resolution in nanoscopy (<10 nm).

**Single-particle averaging**

Computational methods that infer a structure by sorting and averaging data from a large dataset of images showing the same object.

**Epitopes**

Parts of a protein that are detected by an antibody or other binding probe.

**Bio-orthogonal labelling**

Chemical labelling reactions that can occur inside living cells without interfering with endogenous biochemical processes.

supported this view by showing similar Bax assemblies<sup>147</sup> (FIG. 5b). As nanoscopy allows for the immediate visualization of these Bax assemblies in cells, more detailed studies to dissect the exact function, composition and dynamics of these novel structures in the progression of cell death will undoubtedly be performed.

The mitochondrial network of a single human cell contains thousands of copies of mitochondrial DNA (mtDNA), each encoding only 13 subunits of the mitochondrial oxidative phosphorylation system, along with several ribosomal RNA and tRNA species. It came as a surprise when two independent super-resolution studies determined the size of mitochondrial nucleoids as ranging from 70 to 110 nm, which is much smaller than anticipated previously; in addition, the studies revealed wide variability in the shape of these structures<sup>148,149</sup>. Estimates of the mtDNA copy number per nucleoid that were obtained in the pre-super-resolution era indicated values of 2–10 copies of mtDNA per nucleoid<sup>150,151</sup>. With STED nanoscopy, a previously unrecognized clustering of nucleoids was discovered, and this approach therefore allowed a more accurate estimation of the number of nucleoids within a cell<sup>148,152</sup> (FIG. 5c). Combining these numbers with biochemical data revealed that an average of only 1–2 mtDNAs are present within each nucleoid. This finding has far-reaching consequences for modelling the segregation and transmission of mtDNA<sup>153</sup>.

**The labelling challenge**

In fluorescence imaging, the fluorophore attached to a protein of interest is used as a proxy for the localization of the protein. However, this assumption may no longer be valid in nanoscopy, where the distance between a fluorophore and the labelled protein may be larger than the resolution realized in the experiment. Additional challenges stem from incomplete labelling<sup>154</sup>, such as in cases where not all epitopes are decorated. Other undesirable effects of labelling may affect the localization and/or function of the host protein. These effects may become detectable only when cells are imaged at an improved resolution.

In immunocytochemistry, antibodies are frequently used in pairs consisting of a primary antibody that is recognized by several multiple-dye-labelled secondary antibodies. The pairing often provides very good molecular specificity and superior signal-to-noise ratios due to the inherent signal amplification. This advantage over other fluorescent labelling methods comes at the cost of the relatively large size of these binding probes. For example, when attached to a target protein, a pair of IgG antibodies may span up to 15 nm, which is within the resolution regime of nanoscopy (FIG. 6). The use of antigen-binding fragments or of small affinity probes such as aptamers, nanobodies and others, reduces this problem, and some of these probes have been successfully used for nanoscopy<sup>155–157</sup>. Recombinant small binders feature the additional benefit of full experimental reproducibility without the batch-to-batch variation observed with polyclonal antibodies<sup>158</sup>. We predict that antibodies, which represent a vast resource, are to be in use for some time to come. Over the longer term, however, antibodies are likely to be outperformed by small recombinant binders in most nanoscopy applications.

In live-cell nanoscopy, various — often switchable — fluorescent proteins or proteins that facilitate bio-orthogonal labelling with exogenously added fluorophores, such as Snap-tag or Halo-tag, are in use<sup>159–161</sup>. Most of these fusion tags are of similar size (~15–30 kDa). The host proteins that are functionally taggable are generally not directly affected by the size of the tag. The expression levels of the fusion proteins, however, may massively interfere with their nanoscale distributions<sup>162</sup>, and the first examples of using genome editing to address this problem in nanoscopy have been demonstrated<sup>163</sup>.

Although such protein fusions allow close proximity of the fluorophore and the target protein (<3 nm), the fusion protein inescapably adds an extra domain, and the location of the host protein is still not directly reported. A solution might be provided by genetic code expansion in combination with click chemistry. This combination allows site-specific labelling of target proteins by attaching a fluorophore directly to a target protein<sup>164,165</sup> and may even allow investigation of the dynamics of protein subdomains in living cells using nanoscopy. The technical hurdles are still sizeable, but ultimately, this or related methods might be the most adequate approach to address the labelling problems of future nanoscopy.

**Figure 4 | Nanoscopy of neurons.** Investigations into synapse and axon ultrastructure, dendritic spine-neck morphology and aggregation-prone proteins and peptides in neurodegenerative disease have all benefited from the enhanced resolution of nanoscopy. **a** | Actin, spectrin and other proteins form a coordinated quasi-1D lattice structure in neuronal processes. Top and middle: two-colour stochastic optical reconstruction microscopy (STORM) images of axons of fixed cultured rat hippocampal neurons. Top: actin in green, spectrin in magenta. Middle: spectrin in green, adducin in magenta. Bottom: two-colour stimulated emission depletion (STED) imaging of a dendrite stained for spectrin (magenta) and actin (green). Scale bars: 1 μm. **b** | STED nanoscopy revealed that at paranodes (regions flanking the nodal gap), both axonal proteins and glial proteins form periodic quasi-1D arrangements with a high degree of interdependence between the positions of the axonal and the glial proteins. Top: paranode labelled for axonal Caspr and glial neurofascin. Bottom: paranode labelled for the glial proteins ankyrin B and neurofascin. These data suggest the existence of mechanisms that align the cytoskeleton of the axon with that of the glial Schwann cells. Scale bars: 1 μm. **c** | Nanoscopy suggests that synaptic transmission is organized such that the active zone directs action potential-evoked vesicle fusion to occur preferentially at sites directly opposing postsynaptic receptor–scaffold ensembles. In this way, neurotransmitter release is aligned to the corresponding receptors in the postsynaptic cell along ‘nanocolumns’. Top: image of the presynaptic protein Rab3-interacting molecule (RIM) (red) and the postsynaptic scaffolding molecule PSD-95 (blue). Bottom: scheme displaying the concept of ‘nanocolumns’ bridging the synaptic connection between neurons. Scale bar: 200 nm. **d** | Nanoscopy reveals that dendritic spine-neck plasticity regulates compartmentalization of synapses. Examples of fluorescently labelled dendritic spines (top) and their structural plasticity during long-term potentiation (bottom). Scale bars: 500 nm. **e** | Direct observations of fibrils of aggregation-prone mutant huntingtin exon 1 proteins and amyloid-β peptides in cells. These fibrillar aggregates are formed from monomers and potentially higher-order oligomeric conformational species (scheme, left), which can be visualized by nanoscopy. Scale bars: 500 nm. Part **a** (bottom) is adapted with permission from REF. 88, Macmillan Publishers Limited, and (top) from REF. 85. Reprinted with permission from AAAS. Part **b** is adapted with permission from REF. 96, National Academy of Sciences. Schematic of the neuronal cytoskeleton is adapted with permission from REF. 85. Reprinted with permission from AAAS. Part **c** (top) is adapted with permission from REF. 112, Macmillan Publishers Limited. Part **d** is adapted with permission from REF. 118, Macmillan Publishers Limited. Part **e** (top) is adapted with permission from REF. 122, Macmillan Publishers Limited. Part **e** (bottom) is reprinted (adapted) with permission from REF. 121. Copyright (2011) American Chemical Society.

**Genetic code expansion**  
A process that enables the site-specific incorporation of an amino acid that is not among the 20 common proteinogenic amino acids into a protein.

#### Click chemistry

A term that encompasses several chemical reactions that facilitate the fast, specific and irreversible attachment of a probe such as a fluorophore to a specific biomolecule.

#### Getting quantitative

The counting of molecules, which is arguably one of the main goals of molecular analysis with nanoscopy, is a topic of active research. For quantification purposes, all copies of a molecule of interest need to be accounted for, which ties in closely with the challenges associated with labelling. Emerging approaches for such quantitative nanoscopy have made direct use of the single-molecule character of data acquisition in PALM/STORM-type experiments<sup>104,166–170</sup> or in quantitative PAINT (qPAINT)<sup>171</sup> (BOX 1). Alternatively, information

on molecule numbers has been mapped in a coordinate-targeted manner<sup>172</sup> using STED, which has been made possible by analysing the statistics of photon emission events and taking advantage of the fact that any fluorophore can emit only one photon at a time (BOX 1). Quantitative nanoscopy has allowed the number of internalized transferrin receptors to be counted in human cells<sup>172</sup> and the number of flagellar motor proteins to be counted in living bacteria<sup>166</sup>, to name but two examples. The efficiency of labelling as well as environmentally dependent variations in the photophysical

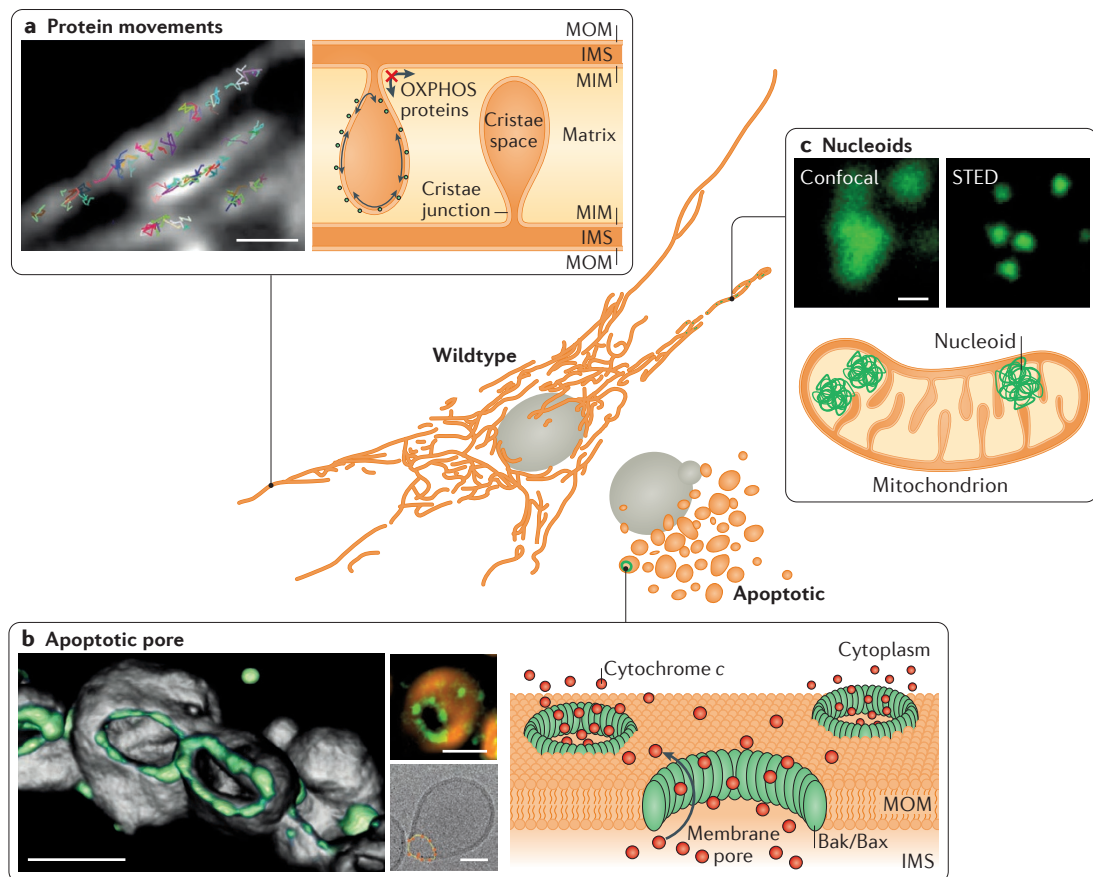
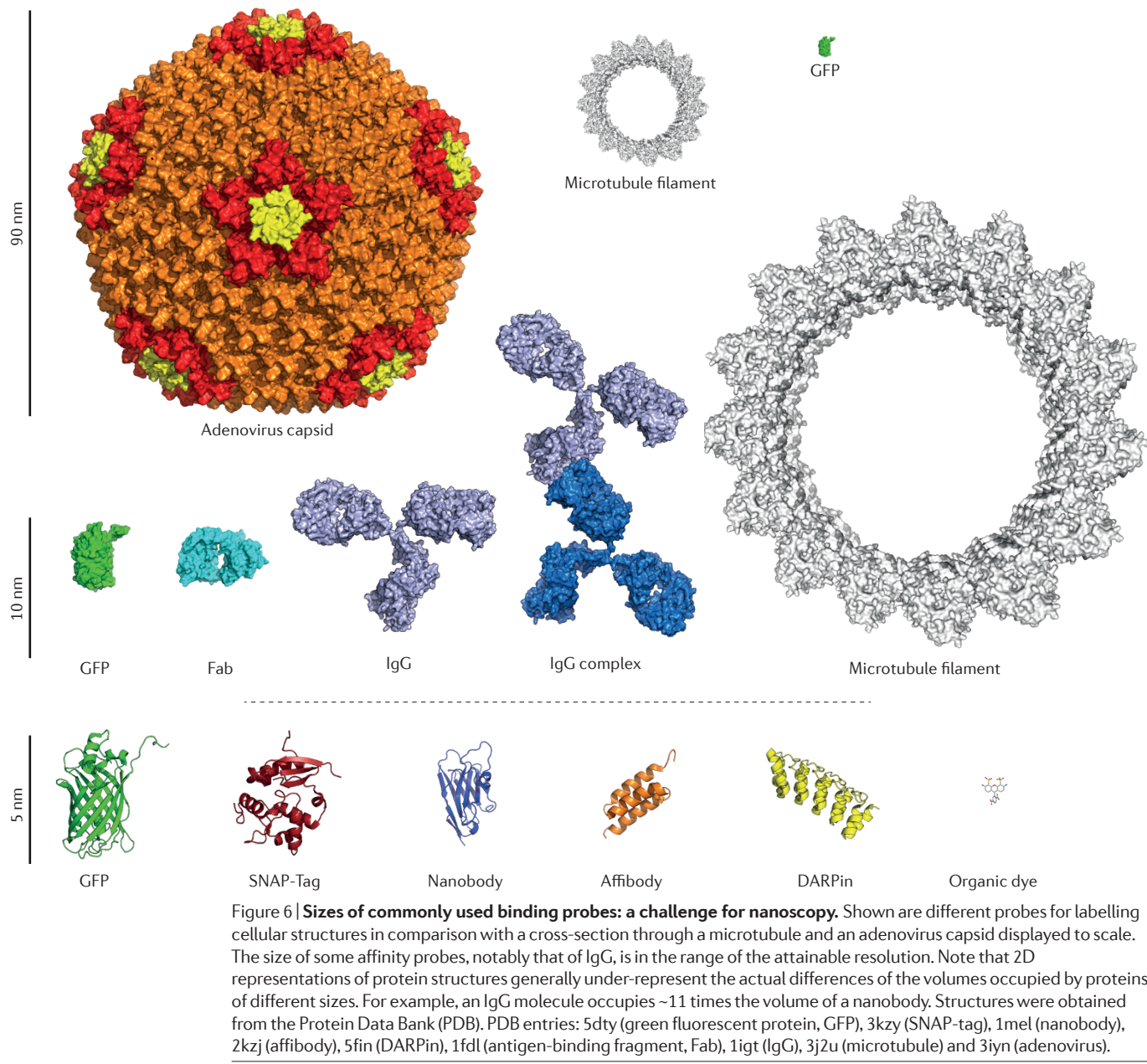


**Figure 5 | Nanoscopy of mitochondria.** Examples of nanoscopy findings in mitochondrial biology. **a** | Movement of the protein complexes that mediate oxidative phosphorylation (OXPHOS) in the mitochondrial inner membrane (MIM) is largely confined to individual cristae. Left panel: recording of the movement of single complex II subunits by single-molecule tracking and localization microscopy. Right panel: schematic showing the confinement of the protein movement within the membrane of a single crista. Scale bar: 1 μm. **b** | The proapoptotic cell-death mediators Bax and Bak were found to form ring-like structures in the mitochondrial outer membrane (MOM) that seem to act as pores to mediate the release of cytochrome c from the mitochondria of apoptotic cells<sup>145,146</sup>. Left panel: 3D reconstruction based on stimulated emission depletion (STED) data of Bax rings formed on apoptotic mitochondria; top, middle: optical section through an apoptotic mitochondrion labelled for Tom20 (red) and Bax (green); bottom, middle: cryo-electron microscopy projection image of a Bax pore in a liposome. Right panel: schematic depicting Bax/Bak pores in the mitochondrial outer membrane. Scale bars: 1 μm (left), 500 nm (top, middle) and 40 nm (bottom, middle). **c** | Knowledge of the number of copies of mitochondrial DNA (mtDNA) molecules in each nucleoid is key for an accurate description of the mtDNA partitioning upon mitochondrial segregation, but previously reported data were inconsistent. A combination of nanoscopy with real-time PCR revealed that most mitochondrial nucleoids in mammalian cells contain only 1 or 2 mtDNAs<sup>148</sup>. Top: nucleoid labelled with an anti-DNA antibody. Comparison between a confocal image and a STED image (S.J., unpublished observations). Bottom: schematic with nucleoids depicted approximately to scale. Scale bar: 200 nm. IMS, intermembrane space. Part **a** is adapted with permission of The Company of Biologists, from REF. 225 (Restricted diffusion of OXPHOS complexes in dynamic mitochondria delays their exchange between cristae and engenders a transitory mosaic distribution. Wilkens, V., Kohl, W. & Busch, K. *J. Cell Sci.* **126**, 103–116, 2013); permission conveyed through Copyright Clearance Center, Inc. Part **b** is adapted from REF 145, CC-BY 4.0, and with permission from REF 147, Macmillan Publishers Limited, and unpublished observations (S.J.).



behaviours of fluorophores both contribute to counting uncertainty and thus complicate these analyses.

While caution needs to be applied when inferring molecule clustering from localization data in coordinate-stochastic methods<sup>173</sup>, a number of strategies to rigorously analyse clustering at the nanoscale have been explored<sup>69,174–176</sup> for PALM and STORM. All these approaches build on the precision (and accuracy) of spatial assignment of fluorophores in the experiment as a key parameter, which must be determined before further analysis. Using the obtained single-molecule coordinates, spatial-point statistical methods have been used to quantify how much the spatial distribution deviates from an entirely uniform distribution of points, giving information on the spatial heterogeneities of protein arrangements<sup>69,174</sup>. A distinct set of so-called

pair correlation methods<sup>175</sup> that make use of mathematical correlation analysis has been used to probe the distribution of localizations relative to all other localizations in their vicinity, thereby providing information on the sizes, densities and abundances of membrane protein clusters.

While cellular nanoscopy imaging of two colours was introduced in early proof-of-concept studies<sup>18,19,57,127,177</sup>, the growing availability of methods for multicolour nanoscopy<sup>23,161,178</sup> will increasingly allow assessment of the relative molecular organizations and interactions of two, three or more species. Established colocalization assessments probing the interaction of two species based on the overlap of their signals in conventional microscopes will need to be reassessed in the age of nanoscale resolution<sup>179</sup>, but a consensus

## Box 1 | Methods of quantitative nanoscopy

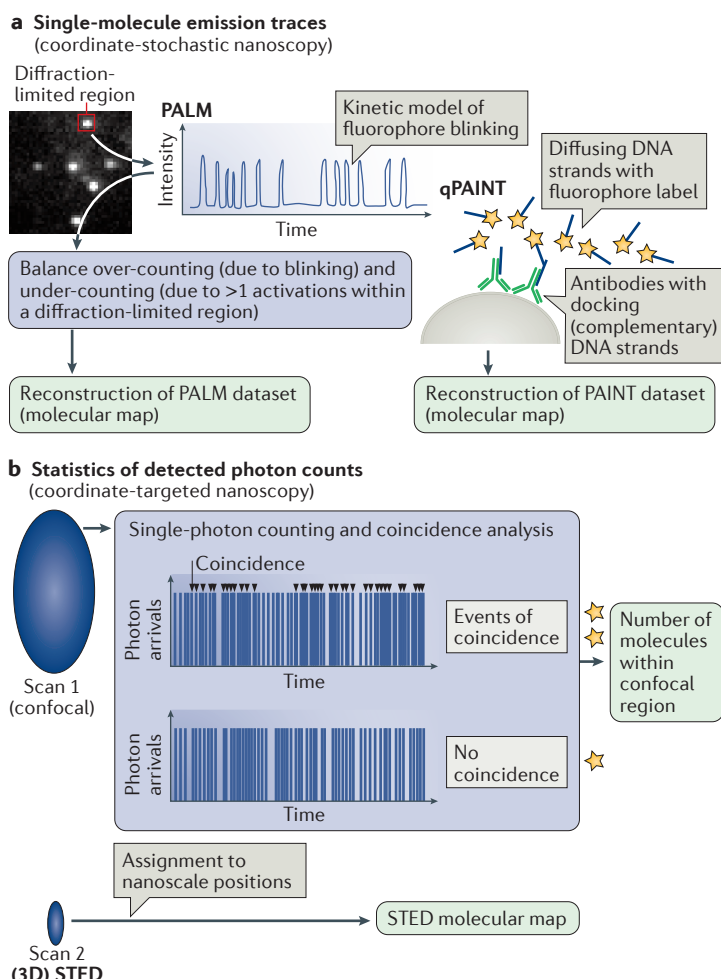
Counting approaches can make direct use of the single-molecule character of fluorophore detection in nanoscopy experiments with photo-activated localization microscopy (PALM), stochastic optical reconstruction microscopy (STORM), ground state depletion with individual molecule return (GSDIM), and quantitative points accumulation for imaging in nanoscale topography (qPAINT). In PALM, for example, a kinetic model of fluorophore blinking is built, and an iterative algorithm adjusts the acceptable time window during which fluorophores can blink to the 'off' state, be dark and still count as one after their return to the bright 'on' state. Thus, fluorophores residing within the localization uncertainty (resolution) can be counted (see figure part a, left). The total number of molecules in a given nanoscale position can also be obtained without analysing the details of blinking over the course of a PALM/STORM-type experiment by using the knowledge of the number of fluorophore localizations obtained under the same conditions from a single fluorophore. Then, taking into account the labelling stoichiometry in the experiment with  $S$  representing the known number (on average) of fluorophores per target molecule, the number of molecules can be estimated by  $N_{\text{molecules}} = N_{\text{localizations}} / (S \cdot N_{\text{localizations for a single fluorophore}})$ . Owing to the uncertainties in the number of blinks within the finite recording time, this approach is especially suitable for obtaining approximate numbers across the whole ensemble of molecular clusters or structures. The qPAINT method (see figure part a, right) relies on well-characterized binding times of fluorophore-carrying DNA imager strands to complementary docking strands. This allows the single-molecule event rate (localizations per unit of time) to be proportional to the number of binding sites present and in effect allows molecular counting. Quantification in nanoscopy can also involve mapping of fluorophore numbers in a coordinate-targeted manner as in stimulated emission depletion (STED) nanoscopy, whereby individual photon emission events are registered. As a molecule cannot emit more than one photon at a time, simultaneous arrival of multiple photons (coincidence) must mean that they originate from multiple fluorophores present within the same region (see the figure part b); thus, their number can be obtained from the analysis of coincidences on multiple detectors.

## Labelling coverage

The fraction of epitopes decorated by a binding probe such as an antibody out of all epitopes potentially available for decoration by this binding probe.

## Fluorescence fluctuation spectroscopy

A set of methods, in particular fluorescence correlation spectroscopy (FCS), which allow the determination of timescales of dynamic processes. By analysing the (self-) similarity (so-called correlations) of the signal from an observed spot over time, information on, for example, molecular diffusion can be obtained.



on 'best practices' is still lacking. Algorithms based on PALM and STORM data to quantify how two species are organized spatially with respect to each other have been implemented<sup>180,181</sup>. As resolution further increases, a suitable analysis method will need to be developed to account for label size, intramolecular flexibility, exact binding locations on a target and overall labelling coverage. In addition, the small numbers of detected photons in some imaging experiments with low copy numbers of molecules of interest and/or fast acquisition times will call for more sophisticated statistical approaches to extract information from raw data.

As for the analysis of processes that occur on short timescales, the STED concept in conjunction with fluorescence fluctuation spectroscopy methods has bridged the gap of high spatial resolution and highest temporal resolution. Use of this combination to map translational diffusion in cell membranes provided unique insights into how the chemical properties of lipids and membrane proteins affect their nanoscale dynamics as well as their local membrane compartmentalization<sup>182–187</sup>. Another powerful approach operating at the single-molecule level that is increasingly applied is the tracking of single molecules within time-lapse datasets from PALM

experiments<sup>188</sup>. This approach allows the creation of spatial maps of molecular movements<sup>142,188,189</sup>. To provide context, these maps can be correlated with imaging data at diffraction-limited or nanoscale resolution to interpret local differences in mobility.

## Nanoscopy goes live

Obtaining reliable nanoscopic data from living cells requires the minimization of disturbances caused by phototoxic effects while maximizing the information obtained from a finite number of available photons. While image acquisition from fixed samples may be compatible with recording times of up to hours, live-cell nanoscopy imposes serious additional challenges. High temporal resolution is required to capture cellular dynamics in 4D, and phototoxicity as well as photo-bleaching limit the useful number of frames that can be recorded. In tissues, further challenges arise, such as elevated autofluorescence and optical aberrations stemming from, for example, large tissue thickness and/or variable local sample composition.

Coordinate-targeted schemes, especially STED with its basic instant light-driven off-switching mechanism, are inherently well suited to the challenge of dynamic

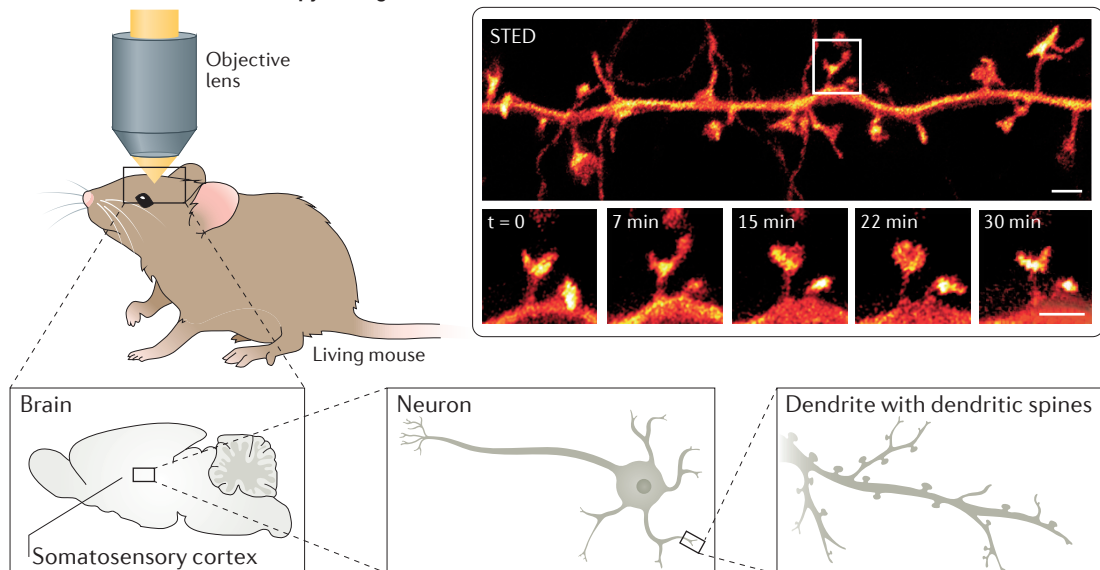
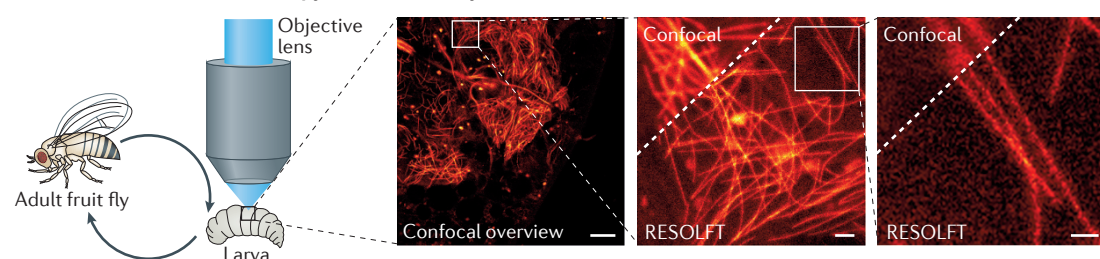
**Dwell time**

Duration for which a scanning nanoscope collects signal at a given position (pixel or voxel).

imaging because they allow high recording speeds<sup>29</sup>. Fast local dynamics in the millisecond range can be captured by limiting the scan range (using a small region of interest (ROI)) and adjusting the effective dwell time to the available signals<sup>67</sup>.

The stochastic nature of PALM, STORM and PAINT approaches sets a minimum time span required to accumulate a representative number of localization events. Hence, with the fluorescent dyes currently used in cellular nanoscopy, recordings with a time window of a few seconds may suffer from an insufficient sampling of the available emitters and an incomplete representation of all the molecules present. Nonetheless, under favourable conditions, video-rate STORM has been demonstrated and used to capture the motion of transferrin receptors in the plasma membrane<sup>66,190</sup>. Importantly, a uniform single-fluorophore event detection rate in

widefield coordinate-stochastic nanoscopy means that the sampling of a structure will proceed evenly throughout the image field. Consequently, properly resolving a large ROI requires as much time as recording a small ROI. This benefit contrasts single-point scanning methods, where the recording time scales linearly with the area (or volume) of the ROI. However, this relation is not insuperable, as STED, RESOLFT and related methods can be implemented in a highly parallelized manner<sup>191–196</sup>. Therefore, these parallelized coordinate-targeted concepts may provide quick acquisition of large ROIs and are predicted to be the methods of choice for future live-cell nanoscopy. Long-term live-cell imaging has already been reported using SIM methods, which also inherently detect in the widefield mode (in parallel) with relatively low light doses applied to samples, albeit not at the resolution attainable by nanoscopy<sup>38,197,198</sup>.

**a In vivo fluorescence nanoscopy through a cranial window in the mouse****b In vivo fluorescence nanoscopy of intact fruit fly larvae**

**Figure 7 | Super-resolution microscopy *in vivo*: mouse and fruitfly nanoscopy.** **a** | Stimulated emission depletion (STED) nanoscopy of a mouse with enhanced yellow fluorescent protein-labelled neurons. Shown are dendritic and axonal details in the molecular layer of the somatosensory cortex of a living, anesthetized mouse. Optical access to the brain cortex was enabled by a cover glass-sealed cranial window. Top panel: image of a neuron. Bottom panel: STED time-lapse recording of spine morphology dynamics. Scale bars: 1 μm. **b** | Reversible saturable/switchable optical linear fluorescence transitions (RESOLFT) imaging of the microtubule cytoskeleton of intact, living *Drosophila melanogaster* larvae. A second instar larva ubiquitously expressing a fusion protein composed of the reversibly switchable fluorescent protein (RSFP) rsEGFP2 fused to α-tubulin was placed under a coverslip and imaged through the intact cuticle. Left: confocal overview. Middle and right: magnifications of the area indicated by the corresponding square. Shown are comparisons of confocal and RESOLFT recordings (separated by a dashed line), exemplifying the difference in resolution. Scale bars: 10 μm, 1 μm and 500 nm (from left to right). Part **a** is adapted from REF. 206. Reprinted with permission from AAAS. Part **b** is adapted with permission from REF. 207, CC-BY 3.0.

Reversibly switchable fluorescent proteins (RSFPs). Fluorescent proteins that can be reversibly switched by light irradiation between long-lived non-fluorescent 'off' and fluorescent 'on' states. RSFPs can be efficiently transferred between the two states at even a low light dose. Because the established state difference remains in place for milliseconds to hours, in RSFP-based reversible saturable/switchable optical linear (fluorescence) transitions nanoscopy, much lower light intensities are needed to break the diffraction barrier than in stimulated emission depletion nanoscopy.

#### Adaptive optics

Optical strategies to compensate for the effects of aberration and ensure more optimal focusing by deliberately modifying the phase across the light wavefront, often in response to a measurement to characterize the presence of aberrations, which is used as feedback.

#### Refractive index

A dimensionless number expressing the factor by which light is slowed down when travelling through a material compared with in vacuum. The refractive index of the immersion medium of an objective lens co-determines its numerical aperture.

Phototoxicity is dependent not only on the light dose, intensity and wavelength but also on the specific fluorophore being used, its immediate environment and the cell type under investigation. There is a general consensus that longer wavelengths and lower light intensities are desirable to reduce unwanted phototoxic effects<sup>199</sup>. The various nanoscopy concepts impose different requirements on the light intensities needed to break the diffraction barrier. STED methods entail relatively high intensities at the maxima of the switching light ( $\sim 1\text{--}200 \text{ MW cm}^{-2}$ ), depending on the desired resolution, albeit only in a single point of the sample at a time. In RESOLFT beam-scanning nanoscopy using reversibly switchable fluorescent proteins, the light intensities used ( $\sim 1\text{--}100 \text{ kW cm}^{-2}$ ) are several orders of magnitude lower and thereby comparable to those typically used in live-cell confocal fluorescence microscopy<sup>199</sup>. Coordinate-stochastic approaches use intensities comparable to those of the coordinate-targeted class ( $\sim 1\text{--}10 \text{ kW cm}^{-2}$  in most experiments). Within the stochastic concepts, light energy is typically deposited continuously to the entire imaged region rather than to a single spot that is swiftly scanned across the specimen. Therefore, the total light dose impinging on the cell is lower by 3–4 orders of magnitude in beam-scanning RESOLFT nanoscopy compared with stochastic single-molecule-based approaches. Still, even these relatively low light doses might be too high for prolonged live-cell nanoscopy, and hence, extended live-cell imaging may ultimately require radically new concepts to overcome the problem of phototoxicity. Potential new approaches on the fluorophore side include dyes and fluorescent proteins that absorb and emit in the infrared range (longer wavelength and lower energy) and/or that are switchable with much lower light intensities. On the instrumentation side, new scanning concepts such as MINFIELD<sup>28</sup> will allow the acquisition of more frames before bleaching, opening new possibilities to address the issue of phototoxicity while maximizing the information gain.

In thicker tissue slices and to an even greater extent in intact organisms, optical readout is complicated by enhanced light absorption and scattering as well as sample-induced optical aberrations with increasing depth of imaging. Strategies from adaptive optics have been explored to alleviate the latter problem for both STED<sup>200,201</sup> and coordinate-stochastic nanoscopy<sup>202</sup>,

although this methodology is still a frontier. In practical terms, careful refractive index matching to the sample is an important first step to reduce aberrations *in vivo*<sup>203</sup>. The growing number of live-cell studies on single cells using various nanoscopy technologies clearly shows that nanoscopy is indeed a powerful and urgently needed tool<sup>92,160,163,190,204</sup>. However, the number of nanoscopy studies focusing on living tissues and intact organisms is still limited to a few proof-of-concept investigations, all of which have used coordinate-targeted schemes<sup>114,116,118,205</sup>. Two examples of nanoscopy in whole animals (mice and fruitfly larvae)<sup>206,207</sup> are presented in FIG. 7.

#### Outlook

We are at a point where an increasing number of platforms for nanoscopy has become accessible to researchers around the world. The capabilities of any nanoscopy method can hardly be captured by a single figure of merit because the rationale of each concept, such as that of STED, STORM or MINFLUX, is much more general than any specific implementation currently available. For example, applying STED with only moderate intensity can readily provide confocal-type recording with extended SIM-like resolution.

Despite the common underlying principles among these methods, the differences in their image generation processes require attention to different challenges. In STED and RESOLFT imaging, adaptation of pixel dwell times and choices in scanning affect the image brightness and contrast. PALM/STORM, PAINT and MINFLUX all require computational image reconstruction. In these methods, aspects such as pixel or voxel binning or the subsets of fluorophore localizations that are included, discarded or combined in postprocessing all affect the image reconstruction outcome.

Carefully applied, however, the promise of fluorescence nanoscopy is immense. Exciting opportunities exist for combining nanoscopy with other imaging modalities, especially electron microscopy. The number of studies in which nanoscopy has been used to obtain new information, either by revealing new details or providing entirely unexpected insights, has overtaken the number of proof-of-principle publications. Nanoscopy, providing a highly resolved view of the cell, prompts new ideas that will help break new ground in cell biology.

1. Abbe, E. Beiträge zur Theorie des Mikroskops und der mikroskopischen Wahrnehmung. *Archiv. Mikrosk. Anat.* **9**, 413–418 (1873).
2. Hell, S. W. & Wichmann, J. Breaking the diffraction resolution limit by stimulated emission: stimulated-emission-depletion fluorescence microscopy. *Opt. Lett.* **19**, 780–782 (1994).
3. Hell, S. W. & Kroug, M. Ground-state-depletion fluorescence microscopy: A concept for breaking the diffraction resolution limit. *Appl. Phys. B* **60**, 495–497 (1995).
4. Hell, S. W. Toward fluorescence nanoscopy. *Nat. Biotechnol.* **21**, 1347–1355 (2003).
5. Hell, S. W. Nanoscopy with focused light (Nobel Lecture). *Angew. Chem. Int. Ed. Engl.* **54**, 8054–8066 (2015).
6. Hell, S. W. Far-field optical nanoscopy. *Science* **316**, 1153–1158 (2007).
7. Gustafsson, M. G. L. Surpassing the lateral resolution limit by a factor of two using structured illumination microscopy. *J. Microsc.* **198**, 82–87 (2000).
8. Klar, T. A., Jakobs, S., Dyba, M., Egner, A. & Hell, S. W. Fluorescence microscopy with diffraction resolution barrier broken by stimulated emission. *Proc. Natl Acad. Sci. USA* **97**, 8206–8210 (2000). First experimental report of fluorescence nanoscopy in a cellular context. Reports STED nanoscopy in a living cell.
9. Donnert, G. *et al.* Macromolecular-scale resolution in biological fluorescence microscopy. *Proc. Natl Acad. Sci. USA* **103**, 11440–11445 (2006).
10. Willig, K. I., Rizzoli, S. O., Westphal, V., Jahn, R. & Hell, S. W. STED microscopy reveals that synaptotagmin remains clustered after synaptic vesicle exocytosis. *Nature* **440**, 935–939 (2006). First application of fluorescence nanoscopy to a biological research question, investigating clustering of the membrane protein synaptotagmin I under different stimulation conditions.
11. Göttfert, F. *et al.* Coaligned dual-channel STED nanoscopy and molecular diffusion analysis at 20 nm resolution. *Biophys. J.* **105**, L01–L03 (2013).
12. Hofmann, M., Eggeling, C., Jakobs, S. & Hell, S. W. Breaking the diffraction barrier in fluorescence microscopy at low light intensities by using reversibly photoswitchable proteins. *Proc. Natl Acad. Sci. USA* **102**, 17565–17569 (2005).
13. Brakemann, T. *et al.* A reversibly photoswitchable GFP-like protein with fluorescence excitation decoupled from switching. *Nat. Biotechnol.* **29**, 942–947 (2011).

14. Grotjohann, T. *et al.* Diffraction-unlimited all-optical imaging and writing with a photochromic GFP. *Nature* **478**, 204–208 (2011). **Refs 13 and 14 provide the first experimental demonstrations of low-light-level RESOLFT nanoscopy in cells.**
15. Betzig, E. *et al.* Imaging intracellular fluorescent proteins at nanometer resolution. *Science* **313**, 1642–1645 (2006).
16. Hess, S. T., Girirajan, T. P. K. & Mason, M. D. Ultra-high resolution imaging by fluorescence photoactivation localization microscopy. *Biophys. J.* **91**, 4258–4272 (2006).
17. Rust, M. J., Bates, M. & Zhuang, X. Sub-diffraction-limit imaging by stochastic optical reconstruction microscopy (STORM). *Nat. Methods* **3**, 793–796 (2006). **Refs 15–17 provide the first demonstrations of the PALM/STORM concept.**
18. Bates, M., Huang, B., Dempsey, G. T. & Zhuang, X. Multicolor super-resolution imaging with photo-switchable fluorescent probes. *Science* **317**, 1749–1753 (2007).
19. Bock, H. *et al.* Two-color far-field fluorescence nanoscopy based on photoswitchable emitters. *Appl. Phys. B* **88**, 161–165 (2007).
20. Egner, A. *et al.* Fluorescence nanoscopy in whole cells by asynchronous localization of photoswitching emitters. *Biophys. J.* **93**, 3285–3290 (2007).
21. Fölling, J. *et al.* Fluorescence nanoscopy by ground-state depletion and single-molecule return. *Nat. Methods* **5**, 943–945 (2008).
22. Heilemann, M. *et al.* Subdiffraction-resolution fluorescence imaging with conventional fluorescent probes. *Angew. Chem. Int. Ed. Engl.* **47**, 6172–6176 (2008).
23. Dempsey, G. T., Vaughan, J. C., Chen, K. H., Bates, M. & Zhuang, X. Evaluation of fluorophores for optimal performance in localization-based super-resolution imaging. *Nat. Methods* **8**, 1027–1036 (2011).
24. Sharonov, A. & Hochstrasser, R. M. Wide-field subdiffraction imaging by accumulated binding of diffusing probes. *Proc. Natl Acad. Sci. USA* **103**, 18911–18916 (2006).
25. Dickson, R. M., Cubitt, A. B., Tsien, R. Y. & Moerner, W. E. On/off blinking and switching behaviour of single molecules of green fluorescent protein. *Nature* **388**, 355–358 (1997). **First report of single-molecule-level switching of a fluorescent protein with light between active and inactive states.**
26. Balzarotti, F. *et al.* Nanometer resolution imaging and tracking of fluorescent molecules with minimal photon fluxes. *Science* **355**, 606–612 (2016). **Reports MINFLUX, a concept for nanometre-level molecule localization and nanoscopy with minimal fluxes of emitted (fluorescence) photons.**
27. Danzl, J. G. *et al.* Coordinate-targeted fluorescence nanoscopy with multiple off states. *Nat. Photonics* **10**, 122–128 (2016).
28. Göttfert, F. *et al.* Strong signal increase in STED fluorescence microscopy by imaging regions of subdiffraction extent. *Proc. Natl Acad. Sci. USA* **114**, 2125–2130 (2017).
29. Westphal, V. *et al.* Video-rate far-field optical nanoscopy dissects synaptic vesicle movement. *Science* **320**, 246–249 (2008).
30. Minsky, M. Microscopy apparatus. US patent 3013467 A (1961).
31. Sheppard, C. J. R. Super-resolution in confocal imaging. *Optik* **80**, 53–54 (1988).
32. Müller, C. B. & Enderlein, J. Image scanning microscopy. *Phys. Rev. Lett.* **104**, 198101 (2010).
33. Chen, B.-C. *et al.* Lattice light-sheet microscopy: Imaging molecules to embryos at high spatiotemporal resolution. *Science* **346**, 1257998 (2014).
34. Hookway, C. *et al.* Microtubule-dependent transport and dynamics of vimentin intermediate filaments. *Mol. Biol. Cell* **26**, 1675–1686 (2015).
35. Hagen, C. *et al.* Structural basis of vesicle formation at the inner nuclear membrane. *Cell* **163**, 1692–1701 (2015).
36. Burnette, D. T. *et al.* A contractile and counterbalancing adhesion system controls the 3D shape of crawling cells. *J. Cell Biol.* **205**, 83–96 (2014).
37. Nixon-Ashell, J. *et al.* Increased spatiotemporal resolution reveals highly dynamic dense tubular matrices in the peripheral ER. *Science* **354**, aaf3928 (2016).
38. Li, D. *et al.* Extended-resolution structured illumination imaging of endocytic and cytoskeletal dynamics. *Science* **349**, aab3500 (2015).
39. Sahl, S. J. *et al.* Comment on “Extended-resolution structured illumination imaging of endocytic and cytoskeletal dynamics”. *Science* **352**, 527 (2016).
40. Dertinger, T., Colyer, R., Iyer, G., Weiss, S. & Enderlein, J. Fast, background-free, 3D super-resolution optical fluctuation imaging (SOFI). *Proc. Natl. Acad. Sci. USA* **106**, 22287–22292 (2009).
41. Geissbuehler, S. *et al.* Live-cell multiplane three-dimensional super-resolution optical fluctuation imaging. *Nat. Commun.* **5**, 5830 (2014).
42. Chen, F., Tillberg, P. W. & Boyden, E. S. Expansion microscopy. *Science* **347**, 543–548 (2015).
43. Harke, B., Ullal, C. K., Keller, J. & Hell, S. W. Three-dimensional nanoscopy of colloidal crystals. *Nano Lett.* **8**, 1309–1313 (2008).
44. Hell, S. & Stelzer, E. H. K. Properties of a 4Pi confocal fluorescence microscope. *J. Opt. Soc. Am. A* **9**, 2159–2166 (1992).
45. Schmidt, R. *et al.* Spherical nanosized focal spot unravels the interior of cells. *Nat. Methods* **5**, 539–544 (2008).
46. Schmidt, R. *et al.* Mitochondrial cristae revealed with focused light. *Nano Lett.* **9**, 2508–2510 (2009).
47. Curdt, F. *et al.* isoSTED nanoscopy with intrinsic beam alignment. *Opt. Express* **23**, 30891–30903 (2015).
48. Böhm, U., Hell, S. W. & Schmidt, R. 4Pi-RESOLFT nanoscopy. *Nat. Commun.* **7**, 10504 (2016).
49. Shtengel, G. *et al.* Interferometric fluorescent super-resolution microscopy resolves 3D cellular ultrastructure. *Proc. Natl. Acad. Sci. USA* **106**, 3125–3130 (2009).
50. Aquino, D. *et al.* Two-color nanoscopy of three-dimensional volumes by 4Pi detection of stochastically switched fluorophores. *Nat. Methods* **8**, 353–359 (2011).
51. Huang, F. *et al.* Ultra-high resolution 3D imaging of whole cells. *Cell* **166**, 1028–1040 (2016). **Comprehensive demonstration of 3D nanoscopy at 10–20 nm resolution across a wide range of cellular structures based on the 4Pi approach (Ref. 44) and its combination with PALM/STORM (Refs 49 and 50).**
52. Huang, B., Wang, W., Bates, M. & Zhuang, X. Three-dimensional super-resolution imaging by stochastic optical reconstruction microscopy. *Science* **319**, 810–813 (2008).
53. Juette, M. F. *et al.* Three-dimensional sub-100 nm resolution fluorescence microscopy of thick samples. *Nat. Methods* **5**, 527–529 (2008).
54. Pavani, S. R. P. *et al.* Three-dimensional, single-molecule fluorescence imaging beyond the diffraction limit by using a double-helix point spread function. *Proc. Natl. Acad. Sci. USA* **106**, 2995–2999 (2009).
55. Lee, H.-I. D., Sahl, S. J., Lew, M. D. & Moerner, W. E. The double-helix microscope super-resolves extended biological structures by localizing single blinking molecules in three dimensions with nanoscale precision. *Appl. Phys. Lett.* **100**, 153701 (2012).
56. Backlund, M. P. *et al.* Simultaneous, accurate measurement of the 3D position and orientation of single molecules. *Proc. Natl. Acad. Sci. USA* **109**, 19087–19092 (2012).
57. Gahlmann, A. *et al.* Quantitative multicolor subdiffraction imaging of bacterial protein ultrastructures in three dimensions. *Nano Lett.* **13**, 987–993 (2013).
58. Jia, S., Vaughan, J. C. & Zhuang, X. Isotropic three-dimensional super-resolution imaging with a self-bending point spread function. *Nat. Photonics* **8**, 302–306 (2014).
59. Shechtman, Y., Sahl, S. J., Backer, A. S. & Moerner, W. E. Optimal point spread function design for 3D imaging. *Phys. Rev. Lett.* **113**, 133902 (2014).
60. Shechtman, Y., Weiss, L. E., Backer, A. S., Lee, M. Y. & Moerner, W. E. Multicolour localization microscopy by point-spread-function engineering. *Nat. Photonics* **10**, 590–594 (2016).
61. Smith, C., Huisman, M., Siemons, M., Grünwald, D. & Stallinga, S. Simultaneous measurement of emission color and 3D position of single molecules. *Opt. Express* **24**, 4996–5013 (2016).
62. Vaughan, J. C., Jia, S. & Zhuang, X. Ultrabright photoactivatable fluorophores created by reductive caging. *Nat. Methods* **9**, 1181–1184 (2012).
63. Xu, K., Babcock, H. P. & Zhuang, X. Dual-objective STORM reveals three-dimensional filament organization in the actin cytoskeleton. *Nat. Methods* **9**, 185–188 (2012).
64. Staudt, T. *et al.* Far-field optical nanoscopy with reduced number of state transition cycles. *Opt. Express* **19**, 5644–5657 (2011).
65. Zhu, L., Zhang, W., Elnatan, D. & Huang, B. Faster STORM using compressed sensing. *Nat. Methods* **9**, 721–723 (2012).
66. Huang, F. *et al.* Video-rate nanoscopy using sCMOS camera-specific single-molecule localization algorithms. *Nat. Methods* **10**, 653–658 (2013).
67. Schneider, J. *et al.* Ultrafast, temporally stochastic STED nanoscopy of millisecond dynamics. *Nat. Methods* **12**, 827–830 (2015).
68. Komis, G., Samajova, O., Ovecka, M. & Samaj, J. Super-resolution microscopy in plant cell imaging. *Trends Plant Sci.* **20**, 834–843 (2015).
69. Williamson, D. J. *et al.* Pre-existing clusters of the adaptor Lat do not participate in early T cell signaling events. *Nat. Immunol.* **12**, 655–662 (2011).
70. Dudok, B. *et al.* Cell-specific STORM super-resolution imaging reveals nanoscale organization of cannabinoid signaling. *Nat. Neurosci.* **18**, 75–86 (2015).
71. Chojnacki, J. *et al.* Maturation-dependent HIV-1 surface protein redistribution revealed by fluorescence nanoscopy. *Science* **338**, 524–528 (2012).
72. Van Engelenburg, S. B. *et al.* Distribution of ESCRT machinery at HIV assembly sites reveals virus scaffolding of ESCRT subunits. *Science* **343**, 653–656 (2014).
73. Bleck, M. *et al.* Temporal and spatial organization of ESCRT protein recruitment during HIV-1 budding. *Proc. Natl. Acad. Sci. USA* **111**, 12211–12216 (2014).
74. Prescher, J. *et al.* Super-resolution imaging of ESCRT-proteins at HIV-1 assembly sites. *PLOS Pathog.* **11**, e1004677 (2015).
75. Hanne, J. *et al.* Stimulated emission depletion nanoscopy reveals time-course of human immunodeficiency virus proteolytic maturation. *ACS Nano* **10**, 8215–8222 (2016).
76. Gahlmann, A. & Moerner, W. E. Exploring bacterial cell biology with single-molecule tracking and super-resolution imaging. *Nat. Rev. Microbiol.* **12**, 9–22 (2014).
77. Chen, C. *et al.* Imaging and intracellular tracking of cancer-derived exosomes using single-molecule localization-based super-resolution microscope. *ACS Appl. Mater. Interfaces* **8**, 25825–25833 (2016).
78. Ilgen, P. *et al.* STED super-resolution microscopy of clinical paraffin-embedded human rectal cancer tissue. *PLOS ONE* **9**, e101563 (2014).
79. Benda, A., Aitken, H., Davies, D. S., Whan, R. & Goldsbury, C. STED imaging of tau filaments in Alzheimer's disease cortical grey matter. *J. Struct. Biol.* **195**, 345–352 (2016).
80. Löschberger, A. *et al.* Super-resolution imaging visualizes the eightfold symmetry of gp210 proteins around the nuclear pore complex and resolves the central channel with nanometer resolution. *J. Cell Sci.* **125**, 570–575 (2012).
81. Szymborska, A. *et al.* Nuclear pore scaffold structure analyzed by super-resolution microscopy and particle averaging. *Science* **341**, 655–658 (2013). **Refs 80 and 81: pioneering studies of NPC architecture by fluorescence nanoscopy employing image-averaging techniques.**
82. Broeken, J. *et al.* Resolution improvement by 3D particle averaging in localization microscopy. *Methods Appl. Fluoresc.* **3**, 014003 (2015).
83. Yang, T. T. *et al.* Superresolution pattern recognition reveals the architectural map of the ciliary transition zone. *Sci. Rep.* **5**, 14096 (2015).
84. Laine, R. F. *et al.* Structural analysis of herpes simplex virus by optical super-resolution imaging. *Nat. Commun.* **6**, 5980 (2015).
85. Xu, K., Zhong, G. & Zhuang, X. Actin, spectrin, and associated proteins form a periodic cytoskeletal structure in axons. *Science* **339**, 452–456 (2013). **Nanoscopy-enabled discovery of a periodic lattice of various cytoskeleton proteins in the axons of neuronal cells.**
86. Zhong, G. *et al.* Developmental mechanism of the periodic membrane skeleton in axons. *eLife* **3**, e04581 (2014).
87. D'Este, E., Kamin, D., Gottfert, F., El-Hady, A. & Hell, S. W. STED nanoscopy reveals the ubiquity of subcortical cytoskeleton periodicity in living neurons. *Cell Rep.* **10**, 1246–1251 (2015).
88. Sidenstein, S. C. *et al.* Multicolour multilevel STED nanoscopy of actin/spectrin organization at synapses. *Sci. Rep.* **6**, 26725 (2016).
89. Bär, J., Kobler, O., van Bommel, B. & Mikhaylova, M. Periodic F-actin structures shape the neck of dendritic spines. **6**, 37136 (2016).
90. Leterrier, C. *et al.* Nanoscale architecture of the axon initial segment reveals an organized and robust scaffold. *Cell Rep.* **13**, 2781–2793 (2015).

91. Leite, S. C. *et al.* The actin-binding protein  $\alpha$ -adducin is required for maintaining axon diameter. *Cell Rep.* **15**, 490–498 (2016).
92. Lukinavicius, G. *et al.* Fluorogenic probes for live-cell imaging of the cytoskeleton. *Nat. Methods* **11**, 731–733 (2014).
93. D'Este, E. *et al.* Subcortical cytoskeleton periodicity throughout the nervous system. *Sci. Rep.* **6**, 22741 (2016).
94. He, J. *et al.* Prevalent presence of periodic actin-spectrin-based membrane skeleton in a broad range of neuronal cell types and animal species. *Proc. Natl Acad. Sci. USA* **113**, 6029–6034 (2016).
95. Albrecht, D. *et al.* Nanoscopic compartmentalization of membrane protein motion at the axon initial segment. *J. Cell Biol.* **215**, 37–46 (2016).
96. D'Este, E., Kamin, D., Balzarotti, F. & Hell, S. W. Ultrastructural anatomy of nodes of Ranvier in the peripheral nervous system as revealed by STED microscopy. *Proc. Natl Acad. Sci. USA* **114**, E191–E199 (2017).
97. Wilhelm, B. G. *et al.* Composition of isolated synaptic boutons reveals the amounts of vesicle trafficking proteins. *Science* **344**, 1023–1028 (2014).
98. Chazeau, A. & Giannone, G. Organization and dynamics of the actin cytoskeleton during dendritic spine morphological remodeling. *Cell. Mol. Life Sci.* **73**, 3053–3073 (2016).
99. Ehmam, N., Sauer, M. & Kittel, R. J. Super-resolution microscopy of the synaptic active zone. *Front. Cell. Neurosci.* **9**, 7 (2015).
100. Kittel, R. J. *et al.* Bruchpilot promotes active zone assembly,  $\text{Ca}^{2+}$  channel clustering, and vesicle release. *Science* **312**, 1051–1054 (2006). **Pioneering study of the molecular organization of presynaptic active zones using fluorescence nanoscopy.**
101. Fouquet, W. *et al.* Maturation of active zone assembly by *Drosophila* Bruchpilot. *J. Cell Biol.* **186**, 129–145 (2009).
102. Owald, D. *et al.* A Syd-1 homologue regulates pre- and postsynaptic maturation in *Drosophila*. *J. Cell Biol.* **188**, 565–579 (2010).
103. Liu, K. S. *et al.* RIM-binding protein, a central part of the active zone, is essential for neurotransmitter release. *Science* **334**, 1565–1569 (2011).
104. Ehmam, N. *et al.* Quantitative super-resolution imaging of Bruchpilot distinguishes active zone states. *Nat. Commun.* **5**, 4650 (2014).
105. Nishimura, H., Badawi, Y., Mori, S. & Shigemoto, K. Dual-color STED microscopy reveals a sandwich structure of Bassoon and Piccolo in active zones of adult and aged mice. *Sci. Rep.* **6**, 27935 (2016).
106. Chamma, I. *et al.* Mapping the dynamics and nanoscale organization of synaptic adhesion proteins using monomeric streptavidin. *Nat. Commun.* **7**, 10773 (2016).
107. Dani, A., Huang, B., Bergan, J., Dulac, C. & Zhuang, X. Superresolution imaging of chemical synapses in the brain. *Neuron* **68**, 843–856 (2010). **STORM analysis of a large number of chemical synapses from different brain regions, quantifying variations in synapse morphology and the distribution of synaptic proteins.**
108. Hoze, N. *et al.* Heterogeneity of AMPA receptor trafficking and molecular interactions revealed by superresolution analysis of live cell imaging. *Proc. Natl Acad. Sci. USA* **109**, 17052–17057 (2012).
109. MacGillivray, H. D., Song, Y., Raghavachari, S. & Blanpied, T. A. Nanoscale scaffolding domains within the postsynaptic density concentrate synaptic AMPA receptors. *Neuron* **78**, 615–622 (2013).
110. Fukata, Y. *et al.* Local palmitoylation cycles define activity-regulated postsynaptic subdomains. *J. Cell Biol.* **202**, 145–161 (2013).
111. Nair, D. *et al.* Super-resolution imaging reveals that AMPA receptors inside synapses are dynamically organized in nanodomains regulated by PSD95. *J. Neurosci.* **33**, 13204–13224 (2013).
112. Tang, A.-H. *et al.* A trans-synaptic nanocolumn aligns neurotransmitter release to receptors. *Nature* **536**, 210–214 (2016).
113. Izeddin, I. *et al.* Super-resolution dynamic imaging of dendritic spines using a low-affinity photoconvertible actin probe. *PLoS ONE* **6**, e15611 (2011).
114. Urban, N. T., Willig, K. I., Hell, S. W. & Nagerl, U. V. STED nanoscopy of actin dynamics in synapses deep inside living brain slices. *Biophys. J.* **101**, 1277–1284 (2011).
115. Chazeau, A. *et al.* Nanoscale segregation of actin nucleation and elongation factors determines dendritic spine protrusion. *EMBO J.* **33**, 2745–2764 (2014).
116. Nagerl, U. V., Willig, K. I., Hein, B., Hell, S. W. & Bonhoeffer, T. Live-cell imaging of dendritic spines by STED microscopy. *Proc. Natl Acad. Sci. USA* **105**, 18982–18987 (2008).
117. Takasaki, K. & Sabatini, B. L. Super-resolution 2-photon microscopy reveals that the morphology of each dendritic spine correlates with diffusive but not synaptic properties. *Front. Neuroanat.* **8**, 29 (2014).
118. Tonnaes, J., Katona, G., Rozsa, B. & Nagerl, U. V. Spine neck plasticity regulates compartmentalization of synapses. *Nat. Neurosci.* **17**, 678–685 (2014). **Reports on the link between nanoscale anatomy and compartmentalization in live spines of mouse brain slices by using time-lapse STED imaging in combination with FRAP measurements, glutamate uncaging, electrophysiology and simulations.**
119. Duim, W. C., Jiang, Y., Shen, K., Fryzman, J. & Moerner, W. E. Super-resolution fluorescence of huntingtin reveals growth of globular species into short fibers and coexistence of distinct aggregates. *ACS Chem. Biol.* **9**, 2767–2778 (2014).
120. Pinotsi, D. *et al.* Direct observation of heterogeneous amyloid fibril growth kinetics via two-color super-resolution microscopy. *Nano Lett.* **14**, 339–345 (2014).
121. Kaminski Schierle, G. S. *et al.* In situ measurements of the formation and morphology of intracellular  $\beta$ -amyloid fibrils by super-resolution fluorescence imaging. *J. Am. Chem. Soc.* **133**, 12902–12905 (2011).
122. Sahl, S. J., Weiss, L. E., Duim, W. C., Fryzman, J. & Moerner, W. E. Cellular inclusion bodies of mutant huntingtin exon 1 obscure small fibrillar aggregate species. *Sci. Rep.* **2**, 895 (2012).
123. Roberti, M. J. *et al.* Imaging nanometer-sized  $\alpha$ -synuclein aggregates by superresolution fluorescence localization microscopy. *Biophys. J.* **102**, 1598–1607 (2012).
124. Sontag, E. M. *et al.* Exogenous delivery of chaperonin subunit fragment ApoCCT1 modulates mutant Huntington cellular phenotypes. *Proc. Natl Acad. Sci. USA* **110**, 3077–3082 (2013).
125. Sahl, S. J. *et al.* Delayed emergence of subdiffraction-limited mutant huntingtin fibrils following inclusion body formation. *O. Rev. Biophys.* **49**, e2 (2016).
126. Li, L. *et al.* Real-time imaging of Huntington aggregates diverting target search and gene transcription. *eLife* **5**, e17056 (2016).
127. Donnert, G. *et al.* Two-color far-field fluorescence nanoscopy. *Biophys. J.* **92**, L67–L69 (2007).
128. Kehrein, K. *et al.* Organization of mitochondrial gene expression in two distinct ribosome-containing assemblies. *Cell Rep.* **10**, 843–853 (2015).
129. Beinlich, F. R., Drees, C., Piehler, J. & Busch, K. B. Shuttling of PINK1 between mitochondrial microcompartments resolved by triple-color superresolution microscopy. *ACS Chem. Biol.* **10**, 1970–1976 (2015).
130. Das, A., Nag, S., Mason, A. B. & Barroso, M. M. Endosome-mitochondria interactions are modulated by iron release from transferrin. *J. Cell Biol.* **214**, 831–845 (2016).
131. French, J. B. *et al.* Spatial colocalization and functional link of purinosomes with mitochondria. *Science* **351**, 733–737 (2016).
132. Huang, B., Jones, S. A., Brandenburg, B. & Zhuang, X. Whole-cell 3D STORM reveals interactions between cellular structures with nanometer-scale resolution. *Nat. Methods* **5**, 1047–1052 (2008).
133. Wurm, C. A., Neumann, D., Schmidt, R., Egner, A. & Jakobs, S. *Sample Preparation for STED Microscopy. In Live Cell Imaging: Methods and Protocols*, Vol. 591 (ed. Papkovsky, D. B.) 185–199 (2010).
134. Wurm, C. A. *et al.* Nanoscale distribution of mitochondrial import receptor Tom20 is adjusted to cellular conditions and exhibits an inner-cellular gradient. *Proc. Natl Acad. Sci. USA* **108**, 13546–13551 (2011).
135. Palade, G. E. The fine structure of mitochondria. *Anat. Rec.* **114**, 427–451 (1952).
136. Shim, S. H. *et al.* Super-resolution fluorescence imaging of organelles in live cells with photoswitchable membrane probes. *Proc. Natl Acad. Sci. USA* **109**, 13978–13983 (2012).
137. Jans, D. C. *et al.* STED super-resolution microscopy reveals an array of MINOS clusters along human mitochondria. *Proc. Natl Acad. Sci. USA* **110**, 8936–8941 (2013).
138. Perkins, G. A. *et al.* The micro-architecture of mitochondria at active zones: electron tomography reveals novel anchoring scaffolds and cristae structured for high-rate metabolism. *J. Neurosci.* **30**, 1015–1026 (2010).
139. Stoldt, S. *et al.* The inner-mitochondrial distribution of Oxa1 depends on the growth conditions and on the availability of substrates. *Mol. Biol. Cell* **23**, 2292–2301 (2012).
140. Sukhorukov, V. M. *et al.* Determination of protein mobility in mitochondrial membranes of living cells. *Biochim. Biophys. Acta* **1798**, 2022–2032 (2010).
141. Dieteren, C. E. J. *et al.* Solute diffusion is hindered in the mitochondrial matrix. *Proc. Natl Acad. Sci. USA* **108**, 8657–8662 (2011).
142. Appelhans, T. *et al.* Nanoscale organization of mitochondrial microcompartments revealed by combining tracking and localization microscopy. *Nano Lett.* **12**, 610–616 (2012).
143. Tait, S. W. & Green, D. R. Mitochondria and cell death: outer membrane permeabilization and beyond. *Nat. Rev. Mol. Cell Biol.* **11**, 621–632 (2010).
144. Nechushtan, A., Smith, C. L., Lamensdorf, L., Yoon, S. H. & Youle, R. J. Bax and Bak coalesce into novel mitochondria-associated clusters during apoptosis. *J. Cell Biol.* **153**, 1265–1276 (2001).
145. Grossé, L. *et al.* Bax assembles into large ring-like structures remodeling the mitochondrial outer membrane in apoptosis. *EMBO J.* **35**, 402–413 (2016).
146. Salvador-Gallego, R. *et al.* Bax assembly into rings and arcs in apoptotic mitochondria is linked to membrane pores. *EMBO J.* **35**, 389–401 (2016). **Refs 145 and 146 are two independent studies reporting on the assembly of Bax in the mitochondrial outer membrane to mediate membrane rupture.**
147. Kuwana, T., Olson, N. H., Kiosses, W. B., Peters, B. & Newmeyer, D. D. Pro-apoptotic Bax molecules densely populate the edges of membrane pores. *Sci. Rep.* **6**, 27299 (2016).
148. Kukat, C. *et al.* Super-resolution microscopy reveals that mammalian mitochondrial nucleoids have a uniform size and frequently contain a single copy of mtDNA. *Proc. Natl Acad. Sci. USA* **108**, 13534–13539 (2011).
149. Brown, T. A. *et al.* Superresolution fluorescence imaging of mitochondrial nucleoids reveals their spatial range, limits, and membrane interaction. *Mol. Cell. Biol.* **31**, 4994–5010 (2011).
150. Iborra, F. J., Kimura, H. & Cook, P. R. The functional organization of mitochondrial genomes in human cells. *BMC Biol.* **2**, 9 (2004).
151. Legros, F., Málka, F., Frachon, P., Lomber, A. & Rojo, M. Organization and dynamics of human mitochondrial DNA. *J. Cell Sci.* **117**, 2653–2662 (2004).
152. Kukat, C. *et al.* Cross-strand binding of TFAM to a single mtDNA molecule forms the mitochondrial nucleoid. *Proc. Natl Acad. Sci. USA* **112**, 11288–11293 (2015).
153. Gustafsson, C. M., Falkenberg, M. & Larsson, N. G. Maintenance and expression of mammalian mitochondrial DNA. *Annu. Rev. Biochem.* **85**, 133–160 (2016).
154. Lau, L., Lee, Y. L., Sahl, S. J., Stearns, T. & Moerner, W. E. STED microscopy with optimized labeling density reveals 9-fold arrangement of a centriole protein. *Biophys. J.* **102**, 2926–2935 (2012).
155. Pleiner, T. *et al.* Nanobodies: site-specific labeling for super-resolution imaging, rapid epitope-mapping and native protein complex isolation. *eLife* **4**, e11349 (2015).
156. Ries, J., Kaplan, C., Platonova, E., Eghlid, H. & Ewers, H. A simple, versatile method for GFP-based super-resolution microscopy via nanobodies. *Nat. Methods* **9**, 582–584 (2012).
157. Mikhaylova, M. *et al.* Resolving bundled microtubules using anti-tubulin nanobodies. *Nat. Commun.* **6**, 7933 (2015).
158. Bradbury, A. & Plückthun, A. Reproducibility: standardize antibodies used in research. *Nature* **518**, 27–29 (2015).
159. Butkevich, A. N. *et al.* Fluorescent rhodamines and fluorogenic carbopyronines for super-resolution STED microscopy in living cells. *Angew. Chem. Int. Ed. Engl.* **55**, 3290–3294 (2016).
160. Bottanelli, F. *et al.* Two-colour live-cell nanoscale imaging of intracellular targets. *Nat. Commun.* **7**, 10778 (2016).
161. Winter, F. R. *et al.* Multicolour nanoscopy of fixed and living cells with a single STED beam and hyperspectral detection. *Sci. Rep.* **7**, 46492 (2017).
162. Gibson, T. J., Seiler, M. & Veitia, R. A. The transience of transient overexpression. *Nat. Methods* **10**, 715–721 (2013).
163. Ratz, M., Testa, I., Hell, S. W. & Jakobs, S. CRISPR/Cas9-mediated endogenous protein tagging for RESOLFT super-resolution microscopy of living human cells. *Sci. Rep.* **5**, 9592 (2015).

164. Nikic, I. & Lemke, E. A. Genetic code expansion enabled site-specific dual-color protein labeling: superresolution microscopy and beyond. *Curr. Opin. Chem. Biol.* **28**, 164–173 (2015).
165. Uttamapinant, C. *et al.* Genetic code expansion enables live-cell and super-resolution imaging of site-specifically labeled cellular proteins. *J. Am. Chem. Soc.* **137**, 4602–4605 (2015).
166. Lee, S.-H., Shin, J. Y., Lee, A. & Bustamante, C. Counting single photoactivatable fluorescent molecules by photoactivated localization microscopy (PALM). *Proc. Natl Acad. Sci. USA* **109**, 17436–17441 (2012).
167. Finan, K., Raulf, A. & Heilemann, M. A set of homooligomeric standards allows accurate protein counting. *Angew. Chem. Int. Ed. Engl.* **54**, 12049–12052 (2015).
168. Puchner, E. M., Walter, J. M., Kasper, R., Huang, B. & Lim, W. A. Counting molecules in single organelles with superresolution microscopy allows tracking of the endosome maturation trajectory. *Proc. Natl Acad. Sci. USA* **110**, 16015–16020 (2013).
169. Rollins, G. C., Shin, J. Y., Bustamante, C. & Pressé, S. Stochastic approach to the molecular counting problem in superresolution microscopy. *Proc. Natl Acad. Sci. USA* **112**, E110–E118 (2015).
170. Hummer, G., Fricke, F. & Heilemann, M. Model-independent counting of molecules in single-molecule localization microscopy. *Mol. Biol. Cell* **27**, 3637–3644 (2016).
171. Jungmann, R. *et al.* Quantitative super-resolution imaging with qPAINT. *Nat. Methods* **13**, 439–442 (2016). **Demonstrates qPAINT, a method for quantitative nanoscopy with low counting error.**
172. Ta, H. *et al.* Mapping molecules in scanning far-field fluorescence nanoscopy. *Nat. Commun.* **6**, 7977 (2015).
173. Annibale, P., Vanni, S., Scarselli, M., Rothlisberger, U. & Radenovic, A. Identification of clustering artifacts in photoactivated localization microscopy. *Nat. Methods* **8**, 527–528 (2011).
174. Truan, Z. *et al.* Quantitative morphological analysis of arrestin2 clustering upon G protein-coupled receptor stimulation by super-resolution microscopy. *J. Struct. Biol.* **184**, 329–334 (2013).
175. Sengupta, P. *et al.* Probing protein heterogeneity in the plasma membrane using PALM and pair correlation analysis. *Nat. Methods* **8**, 969–975 (2011). **Method to analyse complex patterns of protein distributions across the plasma membrane.**
176. Baumgart, F. *et al.* Varying label density allows artifact-free analysis of membrane-protein nanoclusters. *Nat. Methods* **13**, 661–664 (2016).
177. Shroff, H. *et al.* Dual-color superresolution imaging of genetically expressed probes within individual adhesion complexes. *Proc. Natl Acad. Sci. USA* **104**, 20308–20313 (2007). **Early report on the application of two-colour PALM to study pairs of different proteins assembled in adhesion complexes, the central attachment points between the cytoskeleton and the substrate in migrating cells.**
178. Jungmann, R. *et al.* Multiplexed 3D cellular super-resolution imaging with DNA-PAINT and Exchange-PAINT. *Nat. Methods* **11**, 313–318 (2014).
179. Xu, L. *et al.* Resolution, target density and labeling effects in colocalization studies — suppression of false positives by nanoscopy and modified algorithms. *FEMS J.* **283**, 882–898 (2016).
180. Malkusch, S. *et al.* Coordinate-based colocalization analysis of single-molecule localization microscopy data. *Histochemistry and Cell Biology* **137**, 1–10 (2012).
181. Pageon, S. V., Nicovich, P. R., Mollazade, M., Tabarin, T. & Gaus, K. Clus-DoC: a combined cluster detection and colocalization analysis for single-molecule localization microscopy data. *Mol. Biol. Cell* **27**, 3627–3636 (2016).
182. Eggeling, C. *et al.* Direct observation of the nanoscale dynamics of membrane lipids in a living cell. *Nature* **457**, 1159–1162 (2009).
183. Sahl, S. J., Leutenegger, M., Hilbert, M., Hell, S. W. & Eggeling, C. Fast molecular tracking maps nanoscale dynamics of plasma membrane lipids. *Proc. Natl Acad. Sci. USA* **107**, 6829–6834 (2010). **Ref. 182 reports differential diffusion behaviours of phospholipids and sphingolipids in the plasma membranes of living cells, establishing STED-FCS as a powerful tool for live-cell dynamics studies at millisecond timescales, complementary to the fast single-molecule tracking demonstrated in Ref. 183.**
184. Mueller, V. *et al.* STED nanoscopy reveals molecular details of cholesterol- and cytoskeleton-modulated lipid interactions in living cells. *Biophys. J.* **101**, 1651–1660 (2011).
185. Andrade, D. M. *et al.* Cortical actin networks induce spatio-temporal confinement of phospholipids in the plasma membrane — a minimally invasive investigation by STED-FCS. *Sci. Rep.* **5**, 11454 (2015).
186. Saka, S. K. *et al.* Multi-protein assemblies underlie the mesoscale organization of the plasma membrane. *Nat. Commun.* **5**, 4509 (2014).
187. Honigmang, A. *et al.* Phosphatidylinositol 4,5-bisphosphate clusters act as molecular beacons for vesicle recruitment. *Nat. Struct. Mol. Biol.* **20**, 679–686 (2013).
188. Manley, S. *et al.* High-density mapping of single-molecule trajectories with photoactivated localization microscopy. *Nat. Methods* **5**, 155–157 (2008).
189. Das, S. *et al.* Single-molecule tracking of small GTPase Rac1 uncovers spatial regulation of membrane translocation and mechanism for polarized signaling. *Proc. Natl Acad. Sci. USA* **112**, E267–E276 (2015).
190. Jones, S. A., Shim, S. H., He, J. & Zhuang, X. Fast, three-dimensional super-resolution imaging of live cells. *Nat. Methods* **8**, 499–505 (2011).
191. Bingen, P., Reuss, M., Engelhardt, J. & Hell, S. W. Parallelized STED fluorescence nanoscopy. *Opt. Express* **19**, 23716–23726 (2011).
192. Chmyrov, A. *et al.* Nanoscopy with more than 100,000 ‘doughnuts’: *Nat. Methods* **10**, 737–740 (2013).
193. Yang, B., Przybilla, F., Mestre, M., Trebbia, J.-B. & Lounis, B. Large parallelization of STED nanoscopy using optical lattices. *Opt. Express* **22**, 5581–5589 (2014).
194. Bergermann, F., Alber, L., Sahl, S. J., Engelhardt, J. & Hell, S. W. 2000-fold parallelized dual-color STED fluorescence nanoscopy. *Opt. Express* **23**, 211–223 (2015).
195. Chmyrov, A. *et al.* Achromatic light patterning and improved image reconstruction for parallelized RESOLFT nanoscopy. *Sci. Rep.* **7**, 44619 (2017).
196. Hoyer, P. *et al.* Breaking the diffraction limit of light-sheet fluorescence microscopy by RESOLFT. *Proc. Natl Acad. Sci. USA* **113**, 3442–3446 (2016).
197. Shao, L., Kner, P., Rego, E. H. & Gustafsson, M. G. Super-resolution 3D microscopy of live whole cells using structured illumination. *Nat. Methods* **8**, 1044–1046 (2011).
198. York, A. G. *et al.* Instant super-resolution imaging in live cells and embryos via analog image processing. *Nat. Methods* **10**, 1122–1126 (2013).
199. Wäldchen, S., Lehmann, J., Klein, T., van de Linde, S. & Sauer, M. Light-induced cell damage in live-cell super-resolution microscopy. *Sci. Rep.* **5**, 15348 (2015).
200. Patton, B. R. *et al.* Three-dimensional STED microscopy of aberrating tissue using dual adaptive optics. *Opt. Express* **24**, 8862–8876 (2016).
201. Antonello, J., Kromann, E. B., Burke, D., Bewersdorf, J. & Booth, M. J. Coma aberrations in combined two- and three-dimensional STED nanoscopy. *Opt. Lett.* **41**, 3631–3634 (2016).
202. Burke, D., Patton, B., Huang, F., Bewersdorf, J. & Booth, M. J. Adaptive optics correction of specimen-induced aberrations in single-molecule switching microscopy. *Optica* **2**, 177–185 (2015).
203. Willig, K. I. *et al.* Nanoscopy of filamentous actin in cortical dendrites of a living mouse. *Biophys. J.* **106**, L01–L03 (2014).
204. Mo, G. C. H. *et al.* Genetically encoded biosensors for visualizing live-cell biochemical activity at super-resolution. *Nat. Methods* **14**, 427–434 (2017).
205. Testa, I. *et al.* Nanoscopy of living brain slices with low light levels. *Neuron* **75**, 992–1000 (2012).
206. Berning, S., Willig, K. I., Steffens, H., Dibaj, P. & Hell, S. W. Nanoscopy in a living mouse brain. *Science* **335**, 551 (2012).
207. Schnorrerberg, S. *et al.* In vivo super-resolution RESOLFT microscopy of *Drosophila melanogaster*. *eLife* **5**, e15567 (2016).
208. Beliveau, B. J. *et al.* Single-molecule super-resolution imaging of chromosomes and *in situ* haplotype visualization using Oligopaint FISH probes. *Nat. Commun.* **6**, 7147 (2015).
209. Boettiger, A. N. *et al.* Super-resolution imaging reveals distinct chromatin folding for different epigenetic states. *Nature* **529**, 418–422 (2016). **Refs 208 and 209 are pioneering nanoscopy reports using STORM and Oligopaint fluorescence *in situ* hybridization probes on the spatial organization of DNA, including the classification of genomic domains.**
210. Viero, G. *et al.* Three distinct ribosome assemblies modulated by translation are the building blocks of polysomes. *J. Cell Biol.* **208**, 581–596 (2015).
211. Galiani, S. *et al.* Super-resolution microscopy reveals compartmentalization of peroxisomal membrane proteins. *J. Biol. Chem.* **291**, 16948–16962 (2016).
212. Kanchanawong, P. *et al.* Nanoscale architecture of integrin-based cell adhesions. *Nature* **468**, 580–584 (2010). **Early 3D nanoscopy study of the complex nanoscale protein organization within focal adhesions, which are involved in force transmission, cytoskeletal regulation and signalling.**
213. Erdmann, R. S. *et al.* Super-resolution imaging of the Golgi in live cells with a bioorthogonal ceramide probe. *Angew. Chem. Int. Ed. Engl.* **53**, 10242–10246 (2014).
214. Hell, S. W. Microscopy and its focal switch. *Nat. Methods* **6**, 24–32 (2009).
215. Olivier, N., Keller, D., Gonczy, P. & Manley, S. Resolution doubling in 3D-STORM imaging through improved buffers. *PLoS ONE* **8**, e69004 (2013).
216. Lee, Y. L. *et al.* Cby1 promotes Ah1 recruitment to a ring-shaped domain at the centriole–cilium interface and facilitates proper cilium formation and function. *Mol. Biol. Cell* **25**, 2919–2933 (2014).
217. Wang, W., Li, G. W., Chen, C., Xie, X. S. & Zhuang, X. Chromosome organization by a nucleoid-associated protein in live bacteria. *Science* **333**, 1445–1449 (2011).
218. Ptacin, J. L. *et al.* A spindle-like apparatus guides bacterial chromosome segregation. *Nat. Cell Biol.* **12**, 791–798 (2010). **Nanoscopy visualizes components of a dedicated chromosome segregation apparatus in bacterial cells, which features surprising similarities to eukaryotic spindles.**
219. Fu, G. *et al.* *In vivo* structure of the *E. coli* FtsZ-ring revealed by photoactivated localization microscopy (PALM). *PLoS ONE* **5**, e12682 (2010).
220. Lee, M. K., Rai, P., Williams, J., Twieg, R. J. & Moerner, W. E. Small-molecule labeling of live cell surfaces for three-dimensional super-resolution microscopy. *J. Am. Chem. Soc.* **136**, 14003–14006 (2014).
221. Raulf, A. *et al.* Click chemistry facilitates direct labelling and super-resolution imaging of nucleic acids and proteins. *RSC Adv.* **4**, 30462–30466 (2014).
222. Laplante, C., Huang, F., Tebbs, I. R., Bewersdorf, J. & Pollard, T. D. Molecular organization of cytokinesis nodes and contractile rings by super-resolution fluorescence microscopy of live fission yeast. *Proc. Natl Acad. Sci. USA* **113**, E5876–E5885 (2016).
223. Brown, M. S., Grubb, J., Zhang, A., Rust, M. J. & Bishop, D. K. Small Rad51 and Dmc1 complexes often co-occupy both ends of a meiotic DNA double strand break. *PLoS Genet.* **11**, e1005653 (2015).
224. Kaplan, C. *et al.* Absolute arrangement of subunits in cytoskeletal sepin filaments in cells measured by fluorescence microscopy. *Nano Lett.* **15**, 3859–3864 (2015).
225. Wilkens, V., Kohl, W. & Busch, K. Restricted diffusion of OXPHOS complexes in dynamic mitochondria delays their exchange between cristae and engenders a transitory mosaic distribution. *J. Cell Sci.* **126**, 103–116 (2013).

**Acknowledgements**

S.J. and S.W.H. acknowledge funding through the Center for Nanoscale Microscopy and Molecular Physiology of the Brain (CNMPB).

**Competing interests statement**

The authors declare competing interests: see Web version for details.

**Author contributions**

All three authors contributed equally to all four aspects of preparing the article (researching data for the article, substantial contributions to the discussion of the content, writing, and reviewing and editing of the manuscript before submission).

**Publisher's note**

Springer Nature remains neutral with regard to jurisdictional claims in published maps and institutional affiliations.

**SUPPLEMENTARY INFORMATION**

See online article: S1 (box)

ALL LINKS ARE ACTIVE IN THE ONLINE PDF